



RESEARCH ARTICLE

10.1029/2022AV000722

Peer Review The peer review history for this article is available as a PDF in the Supporting Information.

Key Points:

- Subantarctic mode water (SAMW) biogeochemical formation properties are a function of the density of newly formed water
- Newly formed SAMW is undersaturated in oxygen due to opposing effects from cooling (solubility) and entrainment, and air-sea injection
- SAMW is near or above atmospheric $p\text{CO}_2$ during formation and therefore not a strong direct sink of contemporary carbon dioxide

Supporting Information:

Supporting Information may be found in the online version of this article.

Correspondence to:

S. M. Bushinsky,
seth.bushinsky@hawaii.edu

Citation:

Bushinsky, S. M., & Cerovečki, I. (2023). Subantarctic Mode Water biogeochemical formation properties and interannual variability. *AGU Advances*, 4, e2022AV000722. <https://doi.org/10.1029/2022AV000722>

Received 6 APR 2022

Accepted 7 JAN 2023

Author Contributions:

Conceptualization: Seth M. Bushinsky, Ivana Cerovečki

Data curation: Seth M. Bushinsky, Ivana Cerovečki

Formal analysis: Seth M. Bushinsky, Ivana Cerovečki

Funding acquisition: Seth M. Bushinsky, Ivana Cerovečki

Investigation: Seth M. Bushinsky, Ivana Cerovečki

© 2023. The Authors.

This is an open access article under the terms of the [Creative Commons Attribution-NonCommercial License](https://creativecommons.org/licenses/by-nc/4.0/), which permits use, distribution and reproduction in any medium, provided the original work is properly cited and is not used for commercial purposes.

Subantarctic Mode Water Biogeochemical Formation Properties and Interannual Variability

Seth M. Bushinsky¹ and Ivana Cerovečki²

¹Department of Oceanography, School of Ocean and Earth Science and Technology, University of Hawai'i at Mānoa, Honolulu, HI, USA, ²Scripps Institution of Oceanography, University of California San Diego, La Jolla, CA, USA

Abstract Subantarctic mode water (SAMW) is a key water mass for the transport of nutrients, oxygen, and anthropogenic carbon into the ocean interior. However, a lack of biogeochemical observations of SAMW properties during wintertime formation precluded their detailed characterization. Here we characterize for the first time SAMW properties across their entire wintertime formation regions based primarily on biogeochemical profiling floats. Observations show that the SAMW properties differ between the two main formation regions in the Pacific and Indian sectors of the Southern Ocean. SAMW formed in the Pacific is colder, fresher, and higher in oxygen, nitrate, and dissolved inorganic carbon (DIC) than its Indian Ocean counterpart. The relationship between potential density and biogeochemical water properties is nearly identical between the two formation regions; property differences thus predominantly reflect the difference in mean densities of SAMW formed in each region. SAMW is undersaturated in oxygen during formation, which will impact calculations of derived quantities that assume preformed oxygen saturation. SAMW is at or above atmospheric $p\text{CO}_2$ during wintertime and therefore not a direct sink of contemporary carbon dioxide during the formation period. Results from the Biogeochemical Southern Ocean State Estimate suggest anti-correlated interannual variability of DIC, nitrate, and oxygen between the central and southeastern Pacific formation regions similar to previously established patterns in mixed layer physical properties. This indicates that the mean properties of SAMW will vary depending on which sub-region has a stronger formation rate, which is in turn linked to the Southern Annual Mode and the El-Niño Southern Oscillation.

Plain Language Summary In the Southern Ocean, north of the Antarctic Circumpolar Current, wintertime surface ocean heat loss cools the water, increasing its density and forming thick layers of well mixed water that enter the ocean. This water, called Subantarctic Mode Water (SAMW), represents an important pathway for anthropogenic carbon, nutrients and oxygen into the ocean interior. In this study we used new wintertime observations from profiling robots equipped with sensors that measure oxygen, nitrate, and pH in the top 2,000 m to determine important initial properties of SAMW for the first time. We find that the SAMW properties differ between the Pacific and Indian formation regions and are related to the densities of SAMW formed in each basin. These properties indicate that it is unlikely for SAMW to take up present-day carbon dioxide from the atmosphere during formation, though it may still absorb anthropogenic carbon. We investigated how these properties varied year-to-year using an ocean model linked to observations, finding connections between changes in the biogeochemical properties and physical processes as well as large-scale climate variability. These results will provide valuable constraints on interpretation of subsurface ocean measurements and model studies investigating the role of these waters in the global carbon cycle.

1. Introduction

The Southern Ocean (south of 35°S) is responsible for approximately 50% of the contemporary carbon absorbed by the ocean each year (Gruber, Landschützer, & Lovenduski, 2019; Landschützer et al., 2015, 2016). This Southern Ocean contemporary carbon uptake is largely driven by a strong anthropogenic carbon flux (DeVries, 2014; Mikaloff Fletcher et al., 2006) overlaid on a balanced natural carbon cycle (Gruber, Landschützer, & Lovenduski, 2019). North of the Antarctic Circumpolar Current (ACC), the uptake of natural carbon is driven by Thermocline Waters (TW) from the subtropics that cool as they are advected south and are the site of biological production, both of which lower the partial pressure of CO_2 ($p\text{CO}_2$) in the ocean, drawing down carbon from the atmosphere (Gruber, Gloor, et al., 2009; Gruber, Landschützer, & Lovenduski, 2019; Mikaloff Fletcher et al., 2007). This uptake is balanced by the upwelling of Circumpolar Deep Water (CDW) enriched in old carbon from degraded biological material that is released to the atmosphere as CDW reaches the surface south

Methodology: Seth M. Bushinsky, Ivana Cerovečki

Project Administration: Seth M. Bushinsky

Resources: Seth M. Bushinsky, Ivana Cerovečki

Software: Seth M. Bushinsky, Ivana Cerovečki

Validation: Seth M. Bushinsky

Visualization: Seth M. Bushinsky, Ivana Cerovečki

Writing – original draft: Seth M. Bushinsky

Writing – review & editing: Seth M. Bushinsky, Ivana Cerovečki

of the ACC. A fraction of the upwelled CDW is advected southward, where it cools and subducts as Antarctic Bottom Water, while another fraction is advected northward, mixing with TWs advected southward, forming mode and intermediate waters (Iudicone et al., 2011; Morrison et al., 2015). Newly formed Subantarctic Mode Water (SAMW) contains a mix of CDW, Antarctic Intermediate Water (AAIW), older SAMW that is re-entrained as intense surface heat loss during the winter drives deep winter mixed layers and subduction, and TW (Hanawa & Talley, 2001; McCartney, 1977). After subduction, these well-mixed, near-surface layers are advected away from their formation regions into the ocean interior (McCartney, 1977, 1982). SAMW primarily forms in the Indian and Pacific sectors of the Southern Ocean, where wintertime mixed layers are deepest (Figure 1).

After subduction, SAMW is advected by the ACC and can either be re-entrained and modified during subsequent winter mixed layer (ML) deepening or exported into the ocean interior where it is advected by the subtropical gyre circulation (Cerovečki et al., 2019; Hanawa & Talley, 2001; Hartin et al., 2011; Koch-Larrouy et al., 2010; Morrison et al., 2022). SAMW redistributes heat and freshwater from the Southern Ocean to the tropics (Wong et al., 1999) and the export of nutrients from the Southern Ocean through mode and intermediate waters fuels between 44% and 75% of global ocean productivity (Primeau et al., 2013; Sarmiento et al., 2004). SAMW is also one of the major water masses that transports anthropogenic and natural carbon into the ocean interior from the Southern Ocean, based on interior measurements of dissolved inorganic carbon (DIC) and modeling inversion studies (Gruber, Gloor, et al., 2009; Gruber, Landschützer, & Lovenduski, 2019; Mikaloff Fletcher et al., 2006, 2007). Southern Ocean mode and intermediate waters help ventilate the ocean interior with oxygen (Carter et al., 2014; Russell & Dickson, 2003) and their distinctive high oxygen signature is evident as they spread into the subtropical gyre (Hanawa & Talley, 2001; McCartney, 1977). Modeling results indicate that SAMW has accumulated ~20% of the total ocean anthropogenic carbon inventory and gains ~28% of the annual anthropogenic carbon increase, with 60%–86% of the increase coming from air-sea fluxes and the rest accumulated through interior diapycnal processes (Groeskamp et al., 2016; Iudicone et al., 2016). However, the mechanistic understanding of air-sea CO₂ fluxes that we gain from model simulations are dependent on accurate model representation of preformed mode water biogeochemical properties and resulting air-sea fluxes for which validation data has been previously unavailable.

SAMW is not homogeneous in space, but instead consists of pools of water with distinct properties that form in different locations. SAMW is then exported to the subtropics from these well-defined “hotspots” of formation following distinct pathways influenced by topography (Herraiz-Borreguero & Rintoul, 2011; Koch-Larrouy et al., 2010; Li et al., 2021). While many physical processes play an important role in SAMW formation, air-sea buoyancy fluxes and Ekman transport of cold water are generally considered to be dominant (Rintoul & England, 2002; Sloyan & Rintoul, 2001; Speer et al., 2000). SAMW is strongly coupled to the atmosphere and the interannual variability of wintertime atmospheric forcing governs the interannual variability and regional distribution of SAMW formation in the Pacific and Indian sectors of the Southern Ocean, as revealed by Argo observations. In the Southern Hemisphere the extratropical atmospheric circulation has the quasi-stationary zonal wave number 3 (ZW3) pattern present in both the mean atmospheric circulation and its variability on daily, seasonal, and interannual timescales (Raphael, 2004). As SAMW is strongly coupled to the atmosphere, the ZW3 can also be imprinted onto the zonal distribution of deep wintertime mixed layers associated with SAMW formation (Cerovečki & Meijers, 2021; Meijers et al., 2019; Tamsitt et al., 2020). The ZW3 pattern is a prominent feature in the winter quasi-stationary mean sea level pressure (MSLP) anomalies (Cerovečki & Meijers, 2021). The meridional wind anomalies introduced by these MSLP anomalies are of the opposite sign on the two flanks of each center of the MSLP anomaly, resulting in anomalously cold conditions and deep mixed layers on the flank with enhanced southerly winds, and anomalously warm conditions and shallow mixed layers on the flank with enhanced northerly winds. Thus in years with strong wintertime MSLP anomalies in the SAMW formation latitude range, deep wintertime mixed layer depth (MLD) anomalies have a dipole pattern in each of the three ocean sectors, and these MLD anomalies in the three ocean sectors tend to be in phase, which results in a more circumpolar response to the atmospheric forcing (Cerovečki & Meijers, 2021; Tamsitt et al., 2020). Argo observations have also revealed that the variability of mode water volume and properties in SAMW pools is governed not only by local atmospheric forcing, but also by advective processes that transport property anomalies eastward, with a ~1 year lag between the central and southeastern Pacific (Cerovečki et al., 2019; Meijers et al., 2019).

SAMW variability is strongly linked to the dominant modes of variability in the Southern Hemisphere. The Southern Annual Mode (SAM) leads to large-scale wintertime MLD anomalies (Sallée et al., 2010), strongly influencing the volume of subducted mode water. This volume has increased over the Argo period (Gao

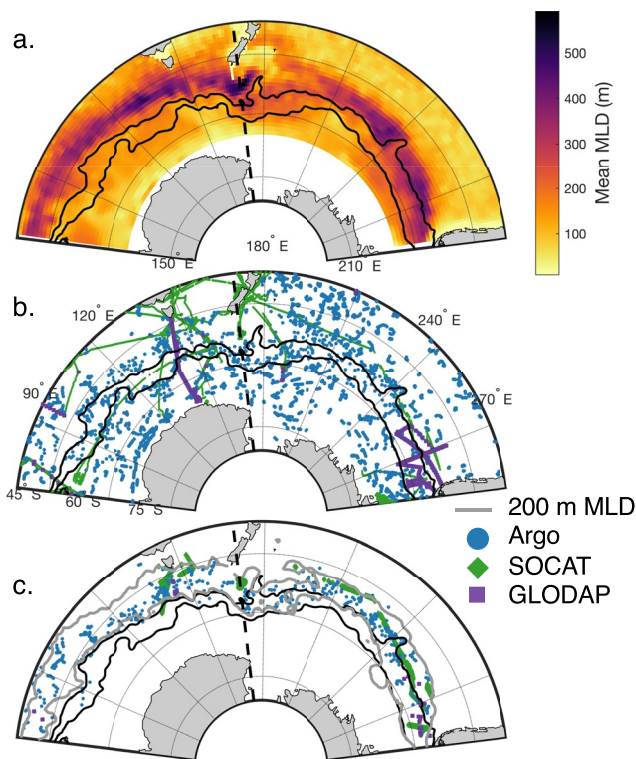


Figure 1. Wintertime mixed layer depths (MLDs) and distribution of wintertime observations in the Indian and Pacific sectors of the Southern Ocean. (a) Mean winter (August–September) MLD calculated from gridded Argo product 2005–2020 (RG-Argo). (b) Map of wintertime water column biogeochemical properties (Argo floats, blue dots; GLODAP data set since 1990, purple squares) and $p\text{CO}_2$ surface measurements (SOCAT data set since 1990, green squares). (c) Same as (b), but only showing data within the SAMW density ranges in the Pacific ($26.8 \leq \sigma_\theta < 27.05 \text{ kg m}^{-3}$) and Indian ($26.6 \leq \sigma_\theta < 26.9 \text{ kg m}^{-3}$) basins within the wintertime MLDs $\geq 200 \text{ m}$. The gray contour represents the mean wintertime 200 m MLD from RG-Argo indicating mode water formation regions. Black lines in all plots are the Polar Front (southern line) and the Subantarctic Front (Orsi et al., 1995). Black dashed line indicates separation between Pacific and Indian basins (170°E).

et al., 2018; Portela et al., 2020) as mixed layers have deepened in response to a strengthening SAM (Qu et al., 2020). In the Pacific, SAMW formation is also influenced by El Niño–Southern Oscillation (ENSO), and the relative phases of the ENSO and SAM govern the interannual variability of SAMW thickness (Meijers et al., 2019).

In contrast to physical properties, changes in large-scale Southern Ocean biogeochemical properties in response to climate variability, including those of SAMW, have primarily been described using the results of model simulations. Modeling studies have linked decreased contemporary Southern Ocean CO_2 fluxes and elevated surface DIC concentrations to positive SAM phase through increased Ekman-driven upwelling of old waters enriched in DIC (Lenton & Matear, 2007; Lovenduski et al., 2007). Verdy et al. (2007) explored climate drivers of oxygen and CO_2 fluxes in the Southern Ocean using a global numerical ocean model. The Pacific dipole described in Meijers et al. (2019) and Cerovečki and Meijers (2021) is evident in the first empirical orthogonal function (EOF) of both oxygen and CO_2 flux variability in Verdy et al. (2007), which the authors also associate with SAM. The upwelling of low oxygen water drives oceanic uptake of oxygen, so the response has the opposite sign from CO_2 . They find that ENSO is a secondary driver of oxygen and CO_2 flux variability in the Pacific, though with a similar magnitude of induced oxygen and CO_2 fluxes and a dipole structure still evident.

Wintertime measurements of biogeochemical tracers in the Southern Ocean are limited, with most of the shipboard measurements that have historically underpinned our understanding of ocean properties concentrated in a few locations (Figure 1). Therefore, despite their importance for determining the distribution of carbon, nutrients, and oxygen in the ocean interior, the biogeochemical properties of SAMW at the time of formation are poorly characterized. Knowing water mass formation properties is key to interpreting downstream biogeochemical measurements and ground-truthing the model-based interpretations of the role of SAMW in nutrient export and anthropogenic carbon uptake. The impact of nutrients exported by SAMW to the global ocean on air-sea carbon dioxide fluxes is determined by whether, once upwelled to the surface, those nutrients are preformed or sourced from biological material that degraded sometime between initial subduction and eventual re-emergence in the upper ocean. Nutrient regeneration from respi-

ration is accompanied by the release of DIC and consumption of oxygen, such that biological production fueled by regenerated nutrients will either be offset by regenerated CO_2 outgassing or will re-fix the regenerated DIC back to organic carbon. Preformed nutrients are not coupled to regenerated DIC and can fuel net carbon uptake from the atmosphere when next upwelled to the surface. Preformed nutrients are often estimated using oxygen measurements, an oxygen consumption to nutrient release respiration ratio, and assumed oxygen saturation during formation. It is therefore important to characterize oxygen and preformed nutrients present in different water masses and to understand if and how they vary in time.

Only one study has analyzed formation properties of SAMW from shipboard measurements made on individual cruises that crossed a SAMW formation region in the southeast Pacific (Carter et al., 2014). Recent deployments of profiling floats equipped with biogeochemical sensors throughout the Southern Ocean by the Southern Ocean Carbon and Climate Observations and Modeling project (SOCCOM; Johnson et al., 2017) offer a new opportunity to characterize these waters and better understand the role that SAMW plays in the global carbon cycle and production.

While mapped interpolation products are available for some biogeochemical variables (Garcia et al., 2010; Landschützer et al., 2013; Lauvset et al., 2016; Rödenbeck et al., 2013) these products are biased toward summertime measurements. For example, inclusion of float-derived $p\text{CO}_2$ with ship-board observations in standard

mapping methods has reduced estimates of the annual Southern Ocean contemporary carbon uptake from an annual uptake of $\sim 1.1 \text{ Pg C yr}^{-1}$ to $0.75 \pm 0.22 \text{ Pg C yr}^{-1}$ (Bushinsky et al., 2019), primarily due to new wintertime observations. Furthermore, the wintertime formation of SAMW has strong temporal and spatial variability, leading to possible biases if properties or variability are extrapolated from too-sparse measurements (Fay et al., 2014). These float-derived year-round, vertically-resolved biogeochemical measurements for the first time enable characterization of these important water masses during formation and will provide the link between surface processes and interior ocean properties and changes. In this study we use wintertime observations from profiling floats and available shipboard measurements to characterize SAMW properties at the time of formation. Using results of an ocean state estimate we determine how these properties vary interannually and regionally prior to export into the global ocean.

2. Methods

2.1. SAMW Identification

SAMW was identified from gridded Argo T&S (hereafter RG-Argo; Roemmich & Gilson, 2009) using a potential vorticity (PV) threshold of $PV < 40 \times 10^{-12} \text{ (m s)}^{-1}$, with PV defined as $PV = f / \rho \partial \sigma_{\theta} / \partial z$, where f is the Coriolis parameter, ρ is the density of seawater, and σ_{θ} is the potential density (taken here to be defined relative to the surface), averaged over the years 2005–2020. This PV threshold was used to identify the density range of core SAMW in the Pacific (170°E to 70°W , 64°S to 45°S) and Indian (68°E to 170°E , 55°S to 30°S) ocean sectors, identified as density bins (0.05 kg m^{-3} -wide spacing) containing at least 5% of total SAMW volume in an annual average. We then used these density ranges throughout the rest of the study to identify wintertime SAMW in each basin.

2.2. Biogeochemical Observations

Biogeochemical properties of the deep wintertime mixed layers that form SAMW were determined from biogeochemical Argo float observations obtained from two sources. The primary data set is observations from over 200 floats equipped with oxygen, nitrate, pH, and bio-optical sensors deployed by SOCCOM since 2014 (May 2021 snapshot; Johnson et al., 2017). The SOCCOM data are supplemented by the University of Washington Argo Oxygen data set (UW Argo O_2 ; v1.1; Drucker & Riser, 2016) that contains post-adjusted Argo oxygen data from 2003 to 2014. Where float data was present in both datasets the SOCCOM data were preferentially used. The final data set contains 311 floats, of which 53 contain profiles that fell within the criteria used to define SAMW formation periods. A profile was determined to have sampled the SAMW formation period if it fell within the density range for a given basin, was from August or September, and had a calculated MLD of at least 200 m.

Oxygen and nitrate in the SOCCOM data set are measured by sensors mounted on the floats with stated uncertainties of $1\text{--}2 \text{ }\mu\text{mol kg}^{-1}$ for oxygen and $<1 \text{ }\mu\text{mol kg}^{-1}$ for nitrate (Johnson et al., 2017). Oxygen uncertainties from the UW Argo O_2 data set are $\sim 1\%$, or $\sim 3 \text{ }\mu\text{mol kg}^{-1}$ at the concentrations observed in this study. The partial pressure of carbon dioxide ($p\text{CO}_2$) and DIC are estimated in the SOCCOM processed data stream from measured pH and an alkalinity multiple linear regression (Carter et al., 2018; Williams et al., 2017) with a theoretical uncertainty of $\sim 11 \text{ }\mu\text{atm}$ for $p\text{CO}_2$, and $\sim 6 \text{ }\mu\text{mol kg}^{-1}$ for DIC (Johnson et al., 2017; Williams et al., 2017, 2018). While float observations underwent prior QC, a secondary QC was performed by checking time series of temperature, salinity, oxygen, nitrate, pH, and derived $p\text{CO}_2$ in the upper 20 m for each float. Large spikes in individual properties with no accompanying changes in related properties were removed from analysis (Table S1 in Supporting Information S1, 116 profiles removed out of 36,247 profiles total).

2.3. Shipboard Observations and Derived Quantities

Shipboard bottle measurements from the Global Ocean Data Analysis Project v2.2020 (GLODAP; Key et al., 2015; Olsen et al., 2016) and underway $p\text{CO}_2$ data from the Surface Ocean CO_2 Atlas v2021 (SOCAT; Bakker et al., 2016) are used to supplement float observations. $p\text{CO}_2$ was calculated from GLODAP DIC and alkalinity using CO2SYS (van Heuven et al., 2011) and the same carbonate system constants as used by the SOCCOM project (Williams et al., 2017). MLDs are calculated for each float and ship profile using a 0.03 kg m^{-3} σ_{θ} change from a 10 m reference (de Boyer Montégut et al., 2004). SOCAT $p\text{CO}_2$ observations are underway

measurements that are not associated with a vertical profile from which MLD could be calculated. Instead, SOCAT observations were matched to the closest $1^\circ \times 1^\circ$ ML from objectively interpolated RG-Argo (Roemmich & Gilson, 2009) MLDs.

$\Delta p\text{CO}_2$ (surface $p\text{CO}_2$ minus atmospheric $p\text{CO}_2$) values were calculated using the atmospheric CO_2 mole fraction ($x\text{CO}_2$, NOAA Greenhouse Gas Marine Boundary Layer Reference; Dlugokencky et al., 2019) matched to the nearest latitude (see Text S2 in Supporting Information S1). A correction for sea level pressure was applied using a mean annual cycle for each location calculated from a 10-year time series of National Centers for Environmental Prediction (NCEP; Kalnay et al., 1996) reanalysis SLP and water vapor pressure calculated from sea surface temperature (SST) and sea surface salinity (Zeebe & Wolf-Gladrow, 2001). Oxygen saturation concentrations are calculated from observed temperature and salinity and García and Gordon (1992) solubility coefficients.

2.4. Biogeochemical Southern Ocean State Estimate (BSOSE)

The biogeochemical Southern Ocean State Estimate (BSOSE; Verdy & Mazloff, 2017) is a coupled biogeochemical-sea-ice-ocean state estimate that assimilates physical and biogeochemical observations, including from biogeochemical profiling floats, creating a coherent picture of Southern Ocean processes that conserves mass and has closed budgets for biogeochemical properties. BSOSE is forced by optimized atmospheric reanalysis fields from ERA-Interim (Dee et al., 2011). We used iteration 135, covering 2013–2019 at $1/6^\circ$ resolution, for analysis of interannual variability. Here we only analyze the spatial and temporal variability of SAMW in BSOSE output from the Pacific sector, where the spatial distribution of deep wintertime MLDs and SAMW formation regions in BSOSE iteration 135 agreed well with those from RG-Argo. The Pacific region was additionally of interest because it reflected the impact of the strong 2015/2016 El Niño.

3. Results and Discussion

3.1. SAMW Formation Properties

The potential density bounds established for regional SAMWs were $26.8 \leq \sigma_\theta < 27.05 \text{ kg m}^{-3}$ in the Pacific sector and $26.6 \leq \sigma_\theta < 26.9 \text{ kg m}^{-3}$ in the Indian sector. These density ranges agree well with those from the literature (e.g., Cerovečki & Meijers, 2021). We identified SAMW properties from float observations in the Pacific and Indian sectors during the time of formation using these density bounds and calculating mean mixed layer properties from August to September at the locations where the float profile MLD was at least 200 m. The depth criterion was used to isolate the deep wintertime mixed layers associated with SAMW formation from other shallower winter mixed layers, such as in areas of reventilation or seasonally formed water that does not connect to the ocean interior (Koch-Larrouy et al., 2010). The threshold value was determined by examining the individual float observations.

Pressure versus time plots of individual floats capture the seasonal cycle of deep mixing in the winter, where the lighter density bound of SAMW outcrops at the surface and newly formed waters bring surface properties into the SAMW layer (Figure 2). As the mixed layer shoals in austral spring, these waters mix in the ocean interior with older SAMW. After leaving Pacific or Indian SAMW formation regions, floats often captured reventilation in other areas, such as float 5904695 that captured moderate wintertime ML deepening in the western Pacific in 2017 (Figure 2). The float was advected eastward by the ACC and captured the process of strong wintertime ML deepening in the Pacific in winters of 2018 and 2019. The subsequent year the float was advected through the Drake Passage into the Atlantic, where SAMW was reventilated, further modifying the properties of SAMW that were set prior to restratification and isolation from the atmosphere. The current study focuses only on the period of deep winter mixed layers and initial formation properties, leaving reventilation and other post-formation modification processes to later work.

Properties in the deep ($>200 \text{ m}$) winter mixed layers were first averaged in density bins within the geographical bounds of each ocean sector and then weighted by volume to calculate mean and standard deviation (Table 1). SAMW formed in the Pacific Ocean is colder and fresher, with higher oxygen, nitrate, DIC, and $p\text{CO}_2$ than SAMW that forms in the Indian Ocean (Table 1, Figures 3a and 3b). The relationship between potential density and each water property is nearly identical between the Pacific and Indian formation regions, indicating that

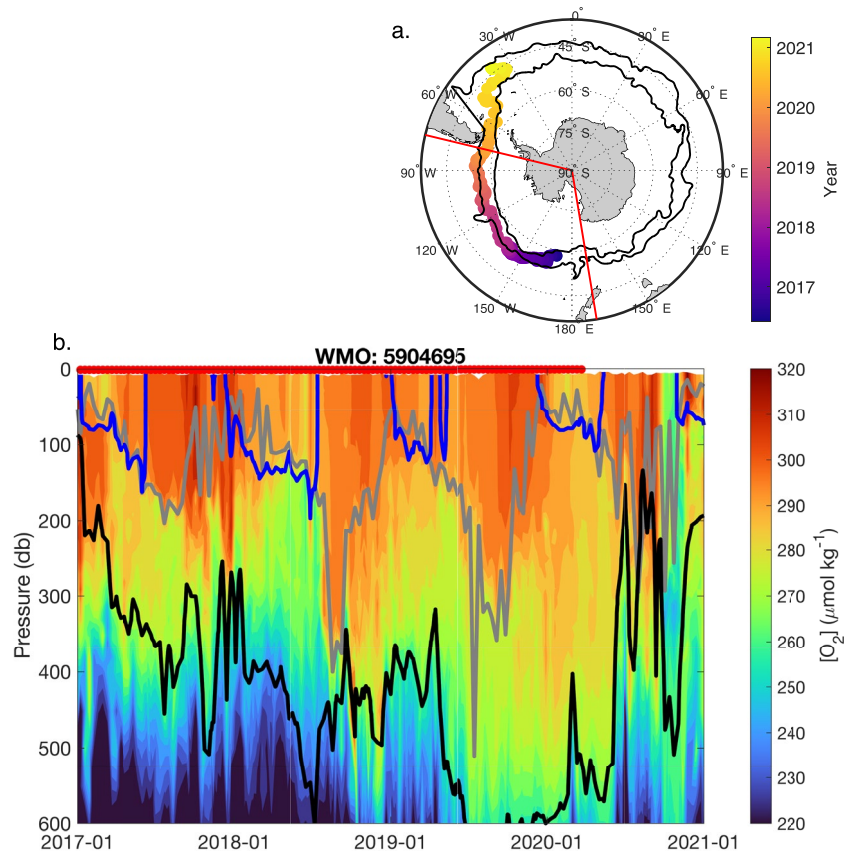


Figure 2. Trajectory and oxygen measurements from float 5904695. (a) Float 5904695 was deployed in the western Pacific in May 2016 and followed the Subantarctic Front (northern black line) as it was advected by the Antarctic Circumpolar Current into the Atlantic basin in 2020. Southern black line is the Polar Front. (b) Float oxygen measurements from the upper 600 m from 2017 to 2021. SAMW density bounds identified for the Pacific are shown for the lighter (blue, 26.8 kg m^{-3}) and denser (black, 27.05 kg m^{-3}) boundaries. MLD (gray) increases in the wintertime and the lighter SAMW boundary outcrops. MLs deeper than 200 m were identified as waters likely to enter the ocean interior and therefore represent SAMW formation waters. This float captured both initial formation (e.g., in 2018 and 2019) as well as what appears to be subsequent reventilation in later years as the float passed into the Atlantic Ocean. The shallow deep SAMW boundary in 2016, 2017, and 2020 (black line) and the relatively shallow MLs indicate that these are not core SAMW formation regions, though there is some ventilation and likely modification of SAMW properties. Red dots above (b) correspond to when the float was in the Pacific sector (red lines in panel a.).

the preformed property differences are primarily a function of the mean potential density of the waters formed in each region (Figure S1 in Supporting Information S1). The relationship between density and ocean properties determined from biogeochemical Argo observations show a generally good agreement with BSOSE for all parameters except surface $p\text{CO}_2$ (Figure 3, light dashed lines). Southern Ocean $p\text{CO}_2$ and the resulting air-sea flux is particularly hard for models to capture due to the non-linear relationship between $p\text{CO}_2$ and SST, DIC, and total alkalinity (Mongwe et al., 2018).

Table 1
Mean and Standard Deviation^a of Preformed Properties in SAMW Formation Regions Obtained From Float Observations

Region	θ ($^{\circ}\text{C}$)	Sal. (PSS-78)	$[\text{O}_2]$ ($\mu\text{mol kg}^{-1}$)	$[\text{NO}_3^-]$ ($\mu\text{mol kg}^{-1}$)	$[\text{DIC}]$ ($\mu\text{mol kg}^{-1}$)	$p\text{CO}_2$ (μatm)
Pacific	5.8 ± 0.6	34.2 ± 0.1	292 ± 6.2	21.5 ± 1.2	2135.1 ± 7.5	419.3 ± 14.4
Indian	9.3 ± 1	34.6 ± 0.2	271 ± 8.2	13.3 ± 2.9	2120 ± 6.3	404.4 ± 10.7

^aMeans and standard deviations are first calculated for each 0.05 kg m^{-3} density bin, then a weighted average is calculated according to the SAMW volume fraction of each bin in the Pacific and Indian regions. The SD represents spatial and interannual variability in addition to measurement error.

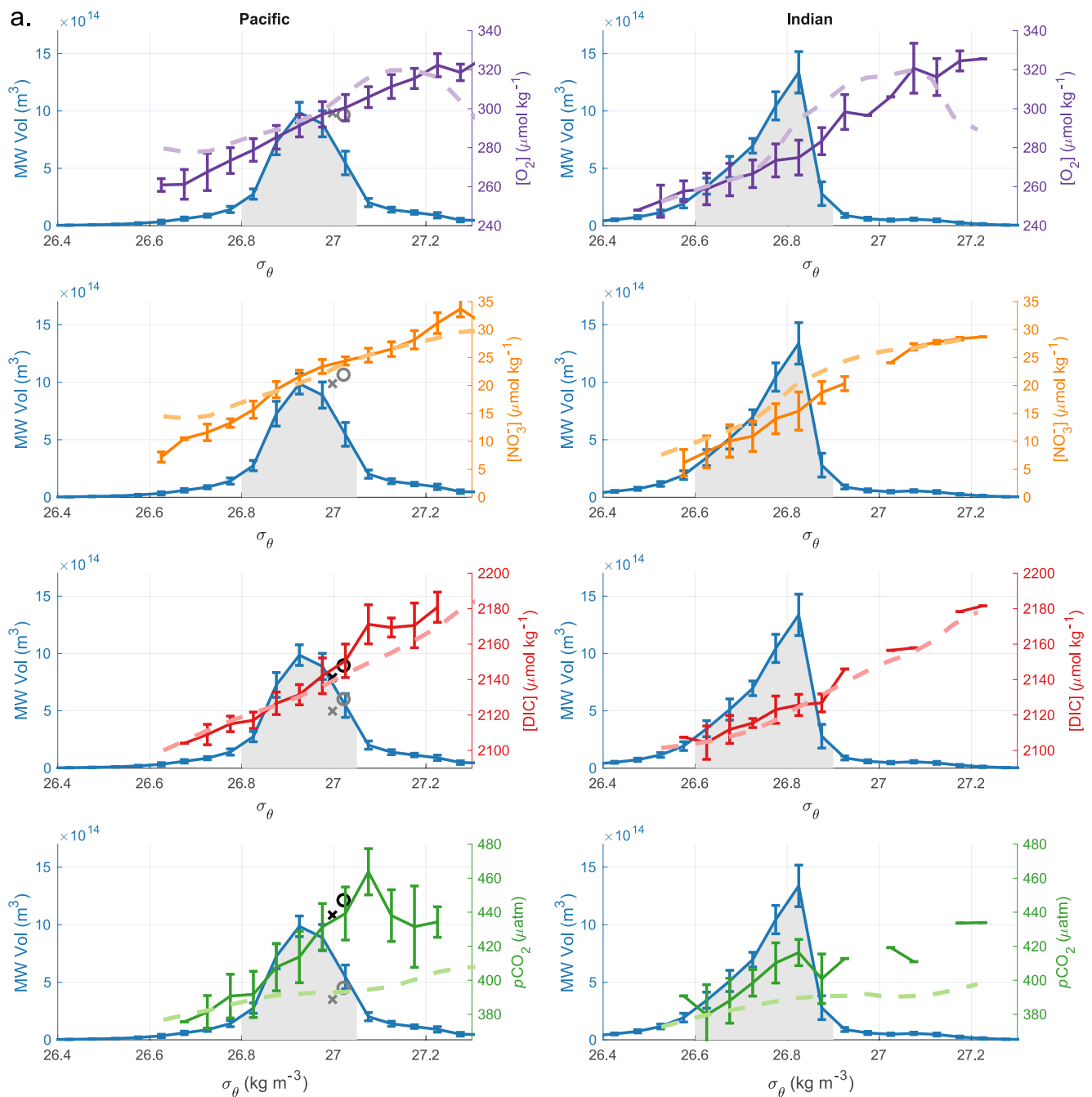


Figure 3. Mixed layer biogeochemical properties of SAMW during wintertime formation and SAMW volume. (a) Mode water volume and oxygen, nitrate, estimated dissolved inorganic carbon (DIC), and $p\text{CO}_2$ are plotted as a function of potential density. The blue curves show the monthly mean volume of water within the ML that satisfies the low potential vorticity (PV) criteria $\text{PV} < 40 \times 10^{-12} \text{ s}^{-1} \text{ m}^{-1}$, obtained from the RG-Argo data set, for months August and September 2005–2020, and binned into 0.05 kg m^{-3} wide density bins with the standard deviations indicating the interannual variability. The shaded areas under the volume curves indicates the density bins that contain at least 5% of SAMW by volume. Colored lines with error bars indicate the average properties ± 1 SD from biogeochemical floats, binned into the same 0.05 kg m^{-3} wide density bins. Volume and property data are from mixed layers that exceed 200 m. Dashed lines are the Aug–Sept mean biogeochemical properties from 5-day averaged output from the Biogeochemical Southern Ocean State Estimate (BSOSE) and time averaged over years 2013–2019 where 5-day averaged MLDs are deeper than 200 m. Overlaid on the Pacific plots are markers indicating the SAMW formation properties identified in Carter et al. (2014) from their “North- Deep Mixed Layer Water” (northwest SAMW outcrop region, gray x’s) and “South-Deep Mixed Layer Water” (southeast SAMW outcrop region, gray o’s) samples. The Carter et al. (2014) $[\text{NO}_3^-]$ is an average of $2.9 \mu\text{mol kg}^{-1}$ lower than this study’s observations in the same density range. Adjusting the Carter et al. (2014) DIC and $p\text{CO}_2$ for the equivalent difference in organic matter (plus change in alkalinity due to organic matter respiration and sea surface temperature difference for $p\text{CO}_2$) yields DIC and $p\text{CO}_2$ shown by the black x’s and o’s. The longitude range of the Indian Ocean sector is $68\text{--}170^\circ\text{E}$, and the Pacific sector $170\text{--}290^\circ\text{E}$. (b) Equivalent to (a) but for potential temperature and salinity.

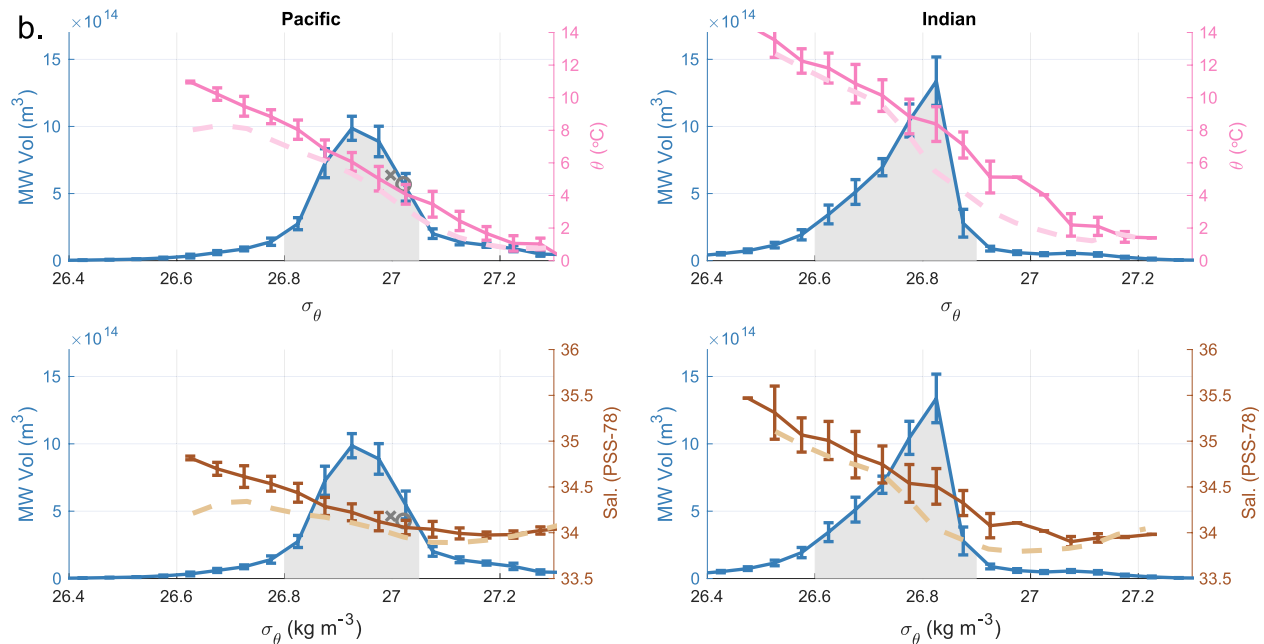


Figure 3. (Continued)

Despite capturing the overall relationship between biogeochemical properties and density shown in Figure 3a, the mean BSOSE properties differ from the Argo observations in some density classes. For instance, while BSOSE falls within the observed variability for oxygen, nitrate, and DIC in the Pacific SAMW density range, in the Indian sector BSOSE oxygen and nitrate are both higher than observations for the denser classes of SAMW. Direct comparison of BSOSE sampled at float profile locations and float observed properties for winter waters with deep ($>200 \text{ m}$) mixed layers within the regional SAMW density ranges indicates mean biases of $-0.001 \pm 0.72^\circ\text{C}$, 0.07 ± 0.12 salinity, $-3.4 \pm 15.5 \mu\text{mol kg}^{-1} [\text{O}_2]$, $1.5 \pm 2.7 \mu\text{mol kg}^{-1} [\text{NO}_3^-]$, and $0.33 \pm 12.1 \mu\text{mol kg}^{-1} [\text{DIC}]$ in the Pacific and $-0.47 \pm 1.19^\circ\text{C}$, -0.02 ± 0.19 salinity, $2 \pm 12.6 \mu\text{mol kg}^{-1} [\text{O}_2]$, $-0.1 \pm 2 \mu\text{mol kg}^{-1} [\text{NO}_3^-]$, and $1.6 \pm 7.5 \mu\text{mol kg}^{-1} [\text{DIC}]$ in the Indian Ocean (upper 200 m average for MLs greater than $200 \text{ m} \pm \text{RMSE}$, Figure S2 in Supporting Information S1). The high RMSE for these comparisons reflects the difficulty for a state estimate to exactly reproduce individual observations, including differences in MLD at a specific location and the related impact on ML properties. The mean biases are small relative to the magnitude of biogeochemical property changes across the SAMW density range. Additionally, in this study we primarily use BSOSE to explore interannual variability (Section 3.4), for which it is more important to reproduce the large-scale density property relationships than to have perfect agreement between every float profile and BSOSE output.

One of the few studies to characterize SAMW and the related AAIW properties in this region used data from a cruise in the winter of 2005 (Carter et al., 2014) to determine deep winter mixed layer properties for the SAMW that forms in the southeast Pacific. The SAMW formation properties described in Carter et al. (2014) fall on the denser end of newly formed SAMW in the Pacific, as expected since the southeast Pacific SAMW is the coldest and freshest. The Carter et al. (2014) estimates are $0.9\text{--}1.4^\circ\text{C}$ colder and $0.05\text{--}0.01$ PSU fresher than the mean Pacific SAMW properties described in this study. Samples of θ , salinity, and $[\text{O}_2]$ fall within ± 1 SD of the property-density relationships described in Figures 3a and 3b (gray symbols in Figure 3). The Carter et al. (2014) $[\text{NO}_3^-]$ is $\sim 2.9 \mu\text{mol kg}^{-1}$ lower than the $[\text{NO}_3^-]$ observed in this study, indicating that either the SAMW formation region sampled in the present study has a greater fraction of older water with a stronger signal of respiration or that less biological production has occurred since that water has been at the surface, either of which could result in a higher $[\text{NO}_3^-]$ value. The $[\text{DIC}]$ and $p\text{CO}_2$ calculated from the Carter et al. (2014) $[\text{DIC}]$ and alkalinity are correspondingly lower than observed values. Correcting for the different amount of biological activity using an assumed Redfield stoichiometry of 106C:16N and recalculating the $[\text{DIC}]$ and $p\text{CO}_2$ (in the latter case, also correcting for SST and the biological impacts on alkalinity) yields values that are within the uncertainty of our observed property relationships with density (Figure 3, black symbols). This indicates that there is no fundamental disagreement between the carbonate system values derived from these float measurements and

those observed by Carter et al. (2014). The $[\text{NO}_3^-]$ and $[\text{DIC}]$ differences between the Carter et al. (2014) results and the current study may additionally indicate variability or change on a multi-year time scale and warrants further exploration with longer time-series of observations or model output. The wide range of biogeochemical properties across the density range of newly formed SAMW illustrates the need for observations that span the entire density and spatial extent of newly formed SAMW to fully characterize properties at the time of formation.

Carter et al. (2021) used ocean observations and interior ocean mixing pathways to estimate preformed properties of oxygen, nitrate, silica, phosphate, and total alkalinity throughout the ocean interior. To compare Carter et al. (2021) to the current values for SAMW we applied the same geographic bounds for the Pacific and Indian regions to the Carter et al. (2021) preformed properties and masked results using the RG-Argo mean winter MLD criteria of >200 m. This yielded preformed properties at 200 m depth of $284.8 \pm 13.3 \mu\text{mol kg}^{-1} [\text{O}_2]$ and $22.3 \pm 3.9 \mu\text{mol kg}^{-1} [\text{NO}_3^-]$ in the Pacific and $257.1 \pm 8.2 \mu\text{mol kg}^{-1} [\text{O}_2]$ and $13.4 \pm 3.6 \mu\text{mol kg}^{-1} [\text{NO}_3^-]$ in the Indian Ocean (mean ± 1 SD). The differences in preformed $[\text{O}_2]$ between Carter et al. (2021) and the current study are of a similar magnitude to our mean SAMW preformed oxygen undersaturation and therefore important to reconcile in future work. Comparison between the results of Carter et al. (2021) and the current study is limited by the lack of density information from the Carter et al. (2021) results, so it is unclear whether the possible bias between these results is meaningful or an artifact of interpretation.

The relative properties of Pacific and Indian formation regions can be broadly interpreted using the property and density relationship described in Figure 3 as differences in mixing fraction of TW and AAIW/CDW in SAMW formation. The Indian SAMW formation region, which is located further north than the formation region in the Pacific, displays a greater influence of TW coming from the subtropics with higher temperatures and lower nutrients and carbon, whereas the Pacific SAMW formation region has a greater influence of upwelled deep water, with high carbon and nutrients, and cold temperatures. Oxygen concentrations follow the north-south temperature gradient, as oxygen air-sea exchange is fast relative to that of CO_2 , allowing the mixed layer to come close to solubility equilibrium with the atmosphere rather than being controlled by the initial $[\text{O}_2]$ of the mixing water masses. This interpretation that preformed biogeochemical properties are dependent on the mixing fraction is consistent with our physical understanding of how mode waters form in these two regions. An early analysis of the Southern Ocean State Estimate found SAMW forming in the Indian Ocean to have a greater fraction of volume transformed from the lighter (TW) waters than the SAMW forming in the Pacific (Cerovečki & Mazloff, 2016). Using data from biogeochemical Argo floats, Fernández Castro et al. (2022) similarly documented the influence of salty, nutrient-poor subtropical waters on SAMW formation properties which decreases from the Indian to Pacific regions and is an important factor influencing the pre-formed nutrient content of SAMW.

The difference between the mean SAMW biogeochemical properties in the Indian and Pacific regions shown in Figure 3a indicates that, at a minimum, properties of newly formed SAMW will change depending on the relative volumes of water formed in the Pacific and Indian SAMW formation regions or within different density classes in the eastern and western areas of each region. During the Argo time period in both the Indian and Pacific sectors of the Southern Ocean, the SAMW volume trends showed a two-layer density structure, with an upper layer volume increase and a lower layer volume decrease (Kolodziejczyk et al., 2019; Portela et al., 2020). The large range of properties within the SAMW density range in each of these two ocean sectors, shown in Figure 3, suggests that this SAMW volume variability is likely accompanied by similar variability of biogeochemical properties. Understanding the link between the density of SAMW formed and the impact on subducted biogeochemical properties may be critical for projection of future Southern Ocean conditions as the predicted poleward intensification of Southern Ocean winds may impact mode water subduction rates differently in the Indian and Pacific formation regions (Downes et al., 2017). While we now have sufficient data to describe the mean SAMW formation properties in the Pacific and Indian Oceans, these basin-wide averages likely mask the intra-basin differences and longer-term variability documented for the physical properties. Current observational coverage alone is of insufficient density and length to convincingly explore intra-basin biogeochemical differences.

3.2. Oxygen Saturation During Formation

SAMW is undersaturated in oxygen at the time of formation in both the Pacific and Indian formation regions (Table 2, Figure 4). Wintertime SAMW $\Delta[\text{O}_2]$, or the observed oxygen concentration minus saturation concentration ($\Delta[\text{O}_2] = [\text{O}_2]_{\text{measured}} - [\text{O}_2]_{\text{saturation}}$, $\mu\text{mol kg}^{-1}$), is negative in almost all individual float observations and in all August and September averages, consistent with the sparse observations available in these wintertime locations in the GLODAP v2.2020 shipboard data set. Pacific SAMW has a mean $\Delta[\text{O}_2]$ of $-11.1 \pm 2.3 \mu\text{mol kg}^{-1}$

Table 2
Mean $\Delta[\text{O}_2]$ and $\Delta p\text{CO}_2$ of SAMW at the Time of Formation

Region	$\Delta[\text{O}_2]$ ($\mu\text{mol kg}^{-1}$) ^a			$\Delta p\text{CO}_2$ (μatm) ^b			
	Argo	GLODAP	Combined Argo and GLODAP	Argo	GLODAP	SOCAT	Combined Argo and SOCAT
Pacific	-11.1 ± 2.3	-12.2 ± 1.7	-11.1 ± 2.3	23.9 ± 14.7	20.1 ± 0.5	5.7 ± 3.6	16.1 ± 14.5
Indian	-7.9 ± 2.4	-6 ± 4.3	-7.7 ± 2.7	9.3 ± 11.7	-14 ± 16.4	-6.4 ± 7.5	0.1 ± 12.2

^a $\Delta[\text{O}_2] = [\text{O}_2]_{\text{ML,observed}} - [\text{O}_2]_{\text{saturation}}$; O_2 saturation calculated as a function of temperature and salinity (García & Gordon, 1992). ^b $\Delta p\text{CO}_2 = p\text{CO}_{2,\text{surf}} - X_{\text{CO}_2} \times \left(\frac{\text{SLP}}{1013.25} - p\text{H}_2\text{O} \right)$; X_{CO_2} from the NOAA Greenhouse Gas Marine Boundary Layer Reference (Dlugokencky et al., 2019), sea level pressure (SLP) in mbar, $p\text{H}_2\text{O}$ calculated as a function of temperature and salinity (Zeebe & Wolf-Gladrow, 2001).

during formation and Indian SAMW has a mean $\Delta[\text{O}_2]$ of $-7.7 \pm 2.7 \mu\text{mol kg}^{-1}$ (Table 2, average of float and GLODAP data). During the formation period, high winds drive strong gas exchange and an oxygen flux into the ocean to relieve undersaturation. $\Delta[\text{O}_2]$ is calculated with an assumption of a standard SLP of 1013.25 mbar (1 atm). Wintertime SLP in the Southern Ocean is typically below 1013.25 mbar and accounting for the mean

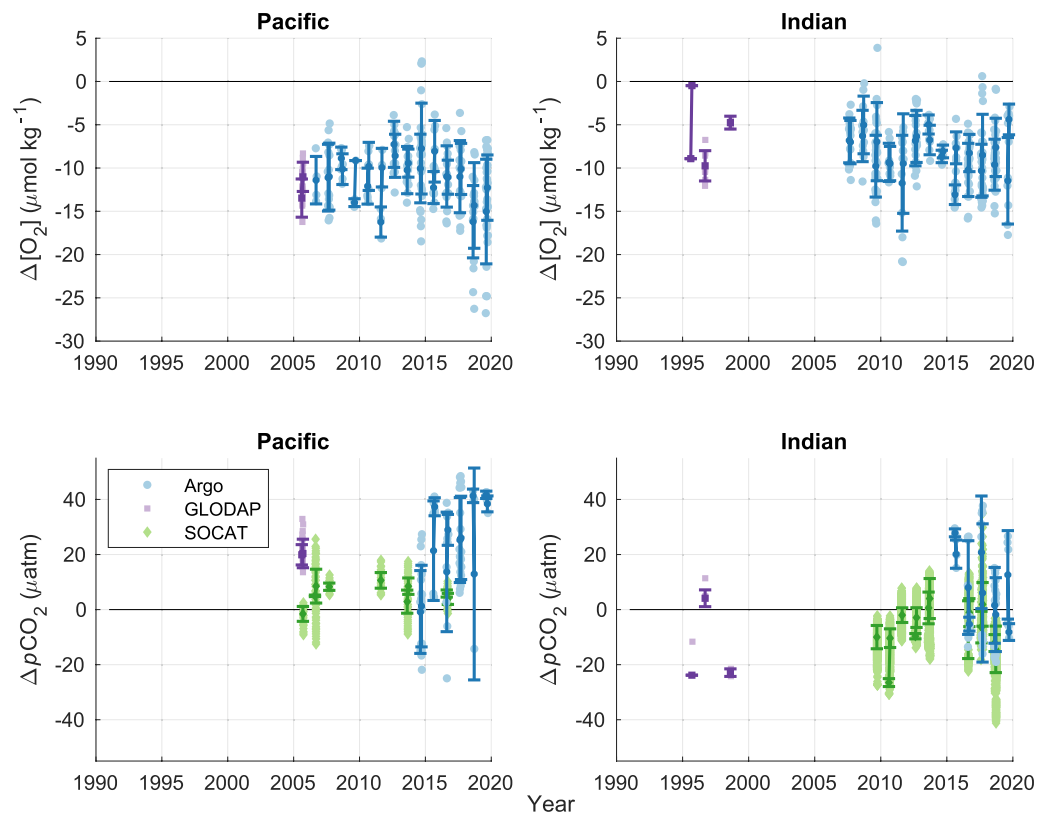


Figure 4. $\Delta p\text{CO}_2$ and $\Delta[\text{O}_2]$ in SAMW formation regions from Argo floats and shipboard observations. (Top row) $\Delta[\text{O}_2]$ is calculated using the mixed layer average oxygen concentration from Argo floats (blue circles) and GLODAP shipboard measurements (purple squares) and is not corrected for local atmospheric pressure, reflecting the use of interior oxygen measurements relative to saturation concentration with an assumed atmospheric pressure of 1 atm. (Bottom row) $\Delta p\text{CO}_2$ values from SOCAT $p\text{CO}_2$ measurements (green diamonds), Argo ph-derived $p\text{CO}_2$ estimates, and GLODAP dissolved inorganic carbon and alkalinity measurements using CO2SYS (van Heuven et al., 2011). SOCAT data are from near-surface underway systems, Argo data from the shallowest observation (typically 5–7 m depth), and GLODAP data are from the upper 25 m due to data availability. $\Delta p\text{CO}_2$ for all data sources were calculated from NOAA ESRL atmospheric CO_2 values, corrected for water vapor pressure, and a 2011–2020 climatological sea level pressure. $\Delta p\text{CO}_2$ from Argo floats is higher (indicates more outgassing or less oceanic uptake) than recent SOCAT $\Delta p\text{CO}_2$ but represents samples made over a wider range of SAMW.

winter SLP in the Pacific and Indian formation regions would reduce oxygen undersaturation by ~30% (Text S4 in Supporting Information S1). The fact that the waters stay undersaturated throughout the wintertime formation period indicates that a combination of surface cooling by atmospheric heat loss and continued entrainment of low oxygen sub-surface waters is maintaining undersaturation throughout the time of water mass formation and subduction.

Undersaturation of oxygen at the time of water mass formation has long been discussed as a source of error in interpreting interior ocean oxygen measurements, but estimates of preformed oxygen undersaturation have primarily come from model results. Model results have indicated significant oxygen undersaturation during deep water formation in the North Atlantic and Southern Ocean (Duteil et al., 2013; Ito et al., 2004). The assumption that water masses are in equilibrium with atmospheric oxygen underpins one of the most common uses of interior ocean oxygen measurements, calculation of apparent oxygen utilization (AOU; $\text{AOU} = [\text{O}_2]_{\text{saturation}} - [\text{O}_2]_{\text{measured}}, \mu\text{mol kg}^{-1}$), where $[\text{O}_2]_{\text{saturation}}$ is determined from temperature and salinity dependent oxygen solubility (García & Gordon, 1992). This quantity is key to determining preformed quantities through the stoichiometric relationship between the consumption of oxygen and release of nutrients and DIC during respiration (e.g., Mackay & Watson, 2021). Oxygen utilization rates (OUR) describe the average respiration in a parcel of water by combining AOU and an age tracer and, again, typically rely on the assumption that preformed oxygen is at saturation. While one study (Koeve & Kähler, 2016) found that undersaturation in preformed oxygen did not make a large difference in calculated oxygen utilization rates due to other offsetting errors, this was based on a single model and did not have the observations to evaluate if that model accurately represented preformed biogeochemical properties.

The increasing number of oxygen-equipped profiling floats deployed throughout the ocean is enabling the first observational studies of wintertime oxygen saturation over large areas. The first basin-scale description of mixed layer $\Delta[\text{O}_2]$ and air-sea oxygen fluxes over several years was also conducted in the Southern Ocean using Argo-oxygen floats, finding broad surface regions of undersaturated wintertime waters but without focusing on specific water masses or ventilation regions (Bushinsky et al., 2017). In the Labrador Sea, Wolf et al. (2018) used Argo-oxygen floats to quantify significant undersaturation in Labrador Sea water at the time of formation that would bias AOU and derived biogeochemical properties. In the study that estimated preformed properties globally (Carter et al., 2021), errors in calculations of AOU were greatest in water formed in the Southern Ocean and in the North Pacific due to the strong degree of wintertime oxygen undersaturation in these regions. Broecker and Peng (1982) introduced the concept of True Oxygen Utilization (TOU), which is the difference between preformed oxygen concentration and the observed concentration, to account for the expected undersaturation during water formation events. Here we show for the first time in SAMW using direct observations of the wintertime formation that SAMW is undersaturated in oxygen when it leaves the ocean surface, altering the interpretation of observations in this water mass throughout the ocean interior and allowing for the calculation of TOU.

It is important to consider oxygen sensor accuracy and method of calibration when comparing to shipboard observations as some float oxygen data have been adjusted to match shipboard data. Oxygen data in the SOCCOM data set (36 out of 53 floats) are calibrated using either atmospheric oxygen as a reference point or using initial shipboard casts if atmospheric data are not available (Johnson et al., 2017; Maurer et al., 2021). Deployments do not occur during the winter and these float oxygen data are therefore independent of the GLODAP shipboard data presented in Figure 4 and Table 2. Oxygen data in the UW Argo O_2 data set are re-processed using a two-point correction (one near-surface and one deep calibration value). The near-surface values are air measurements (if available) or World Ocean Database (WOD, Garcia et al., 2010) mean values. Surface reference values for the WOD were only used if the water was close to saturation (98%–101% O_2 saturation). It is therefore unlikely that any of the shipboard observations shown in Figure 4 were used in the calibration. Therefore, while the uncertainty of oxygen data corrected to WOD is higher than air-calibrated data, these also represent independent observations from the GLODAP data. Uncertainties for the SOCCOM (1–2 $\mu\text{mol kg}^{-1}$) and UW Argo O_2 (~3 $\mu\text{mol kg}^{-1}$) datasets are much smaller than the mean offset and SD of the data shown here and are therefore unlikely to be a major factor in the undersaturation found in the pre-formed oxygen estimates.

3.3. Carbon Dioxide Saturation During Formation

Mean monthly derived $\Delta p\text{CO}_2$ (surface $p\text{CO}_2$ minus atmospheric $p\text{CO}_2$, Text S2 in Supporting Information S1) determined only from float observations is positive in the Pacific ($22.5 \pm 13.5 \mu\text{atm}$) formation region and

slightly positive in the Indian SAMW formation region ($9.5 \pm 12.9 \mu\text{atm}$) (Table 2; Figure 4, bottom). In both the Pacific and Indian SAMW formation regions the $\Delta p\text{CO}_2$ calculated from float observations overlaps with, but is generally higher than, either direct shipboard measurements (SOCAT) or derived $\Delta p\text{CO}_2$ from paired DIC and alkalinity measurements (GLODAP). SOCAT $p\text{CO}_2$ observations are direct measurements with accuracy better than $5 \mu\text{atm}$ (including quality flags A-D, Lauvset et al., 2017), while the float-derived $p\text{CO}_2$ estimates utilize a recently developed technique with a theoretical uncertainty of approximately $\pm 11 \mu\text{atm}$ (Williams et al., 2017). Float observations have previously shown higher $p\text{CO}_2$ during the winter than has been recorded in the SOCAT database (Gray et al., 2018; Williams et al., 2018). This elevated wintertime $p\text{CO}_2$ yields a reduction in the Southern Ocean (south of 35°S) CO_2 sink in 2015–2017 from 1.1 Pg C yr^{-1} based on SOCAT data alone to $0.75 \text{ Pg C yr}^{-1}$ using a combined SOCAT and SOCCOM data set (Bushinsky et al., 2019). These results have been challenged, most recently by a study using atmospheric CO_2 measurements and atmospheric transport models to constrain the Southern Ocean sink (Long et al., 2021), which yielded a stronger Southern Ocean CO_2 sink, though with overlapping uncertainties between the atmospheric constraint and the SOCCOM and SOCAT float-based $p\text{CO}_2$ estimates in all months for which atmospheric data existed and potential complications from previously documented interannual and decadal variability.

The key question for average values of $\Delta p\text{CO}_2$ or air-sea fluxes is whether averaged float estimates of $p\text{CO}_2$ are accurate, not whether individual observations are precise. Crossover comparisons between ship and float $p\text{CO}_2$ have indicated a possible high bias of float $p\text{CO}_2$ by $\sim 4 \mu\text{atm}$ (Fay et al., 2018; Gray et al., 2018; Williams et al., 2018), smaller than the differences between the Argo and SOCAT mean values in Table 2. An updated crossover comparison with the addition of a filter eliminating crossover density differences $> 0.03 \text{ kg m}^{-3}$ yields a mean float-derived $p\text{CO}_2$ bias of $-1.86 \pm 15.8 \mu\text{atm}$ (SOCAT minus floats, $n = 52$, Figure S3 in Supporting Information S1). Recent work evaluating float $p\text{CO}_2$ against shipboard observations indicates that float $p\text{CO}_2$ may be high by $\sim 6 \mu\text{atm}$ (Mackay & Watson, 2021; Wu et al., 2022) and comparison against aircraft-derived CO_2 fluxes indicate that float-derived outgassing is too strong in the winter due to high-biased $p\text{CO}_2$ values. A possible bias of up to $6 \mu\text{atm}$ makes it unlikely that an error in the $p\text{CO}_2$ estimation method is responsible for the entire $17\text{--}20 \mu\text{atm}$ difference in $\Delta p\text{CO}_2$ between the mean Argo and SOCAT values shown in Figure 4, though it may be responsible for some of the offset.

A large portion of the difference between the SAMW formation $\Delta p\text{CO}_2$ from SOCAT and Argo is more likely due to the differences in sample distribution within each of these formation regions. The strong coupling of density and biogeochemical properties seen in Figure 3 highlights the importance of sampling the full range of densities. Previous work demonstrating spatial variability in physical formation properties of SAMW indicates that spatial variations in biogeochemical properties are also likely to exist. Histograms of the relative frequency of $\Delta p\text{CO}_2$, longitude, σ_θ , and θ of mode water formation region observations by the Argo and SOCAT datasets identify differences in the sample distributions of these observations (Figure 5). In the Pacific, SOCAT-determined $\Delta p\text{CO}_2$ has a peak of $\sim 0 \mu\text{atm}$ and a tail toward positive values. The SOCAT observations are primarily from $\sim 170^\circ\text{E}$, at the very western edge of the Pacific basin, while one cruise crossed the Pacific in 2006. This results in observations that are primarily from σ_θ $26.88\text{--}26.9 \text{ kg m}^{-3}$ and θ of $7.26\text{--}7.94^\circ\text{C}$. Float observations cover a broader range of locations within the Pacific and are consequently spread more evenly across the SAMW density range. SOCAT sample coverage in the Indian Ocean is primarily from cruises originating from Tasmania and do not cover the large formation regions in the central and western Indian Ocean. There are relatively few GLODAP-derived $\Delta p\text{CO}_2$ values in either basin, so our best estimate of the $\Delta p\text{CO}_2$ for each region is an average of monthly values from the SOCAT and Argo datasets, yielding $16.1 \pm 14.5 \mu\text{atm}$ $\Delta p\text{CO}_2$ in the Pacific and $0.1 \pm 12.2 \mu\text{atm}$ $\Delta p\text{CO}_2$ in the Indian Ocean. If we applied a uniform $6 \mu\text{atm}$ bias to the float-derived $p\text{CO}_2$ values, it would lower the mean $\Delta p\text{CO}_2$ at formation to $12.7 \pm 12.8 \mu\text{atm}$ in the Pacific and $-3.1 \pm 10.7 \mu\text{atm}$ in the Indian Ocean.

The entire Southern Ocean is a significant sink for contemporary carbon, mainly driven by the increase in atmospheric anthropogenic carbon and resulting oceanic anthropogenic uptake (DeVries, 2014; Gruber, Gloor, et al., 2009; Mikaloff Fletcher et al., 2006). Much of this anthropogenic carbon is both stored in and exported by mode and intermediate waters (Álvarez et al., 2009; Gruber, Doney, et al., 2009; Mikaloff Fletcher et al., 2006; Sabine and Tanhua, 2010; Sabine et al., 2004). Model-derived calculations of anthropogenic carbon uptake use the difference in ocean carbon fluxes and accumulation between model runs that do and do not include increasing atmospheric carbon to determine uptake rates of anthropogenic carbon (Groeskamp et al., 2016; Iudicone et al., 2011, 2016). This approach relies on an accurate representation of water mass properties and the physical and biogeochemical processes that influence the carbonate system in models, which have been shown to

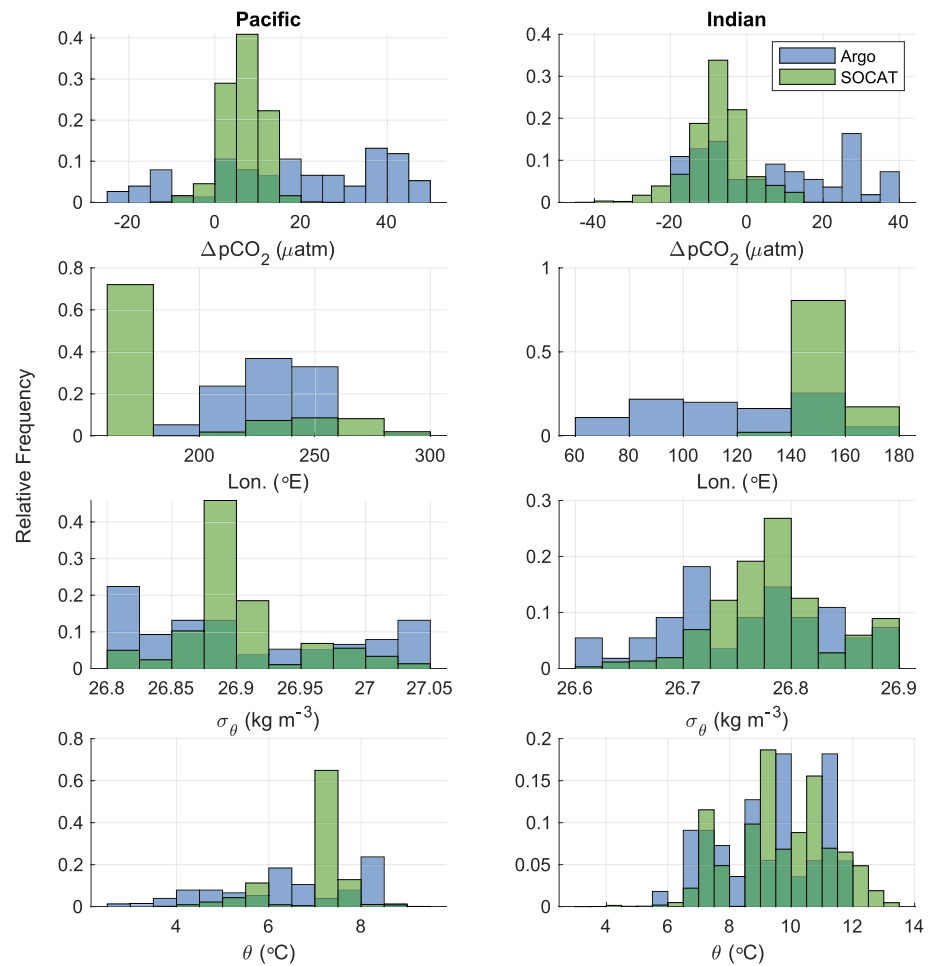


Figure 5. Properties associated with $\Delta p\text{CO}_2$ calculated from SOCAT and Argo. Relative frequency histograms of calculated $\Delta p\text{CO}_2$ and the associated longitude, potential density, and potential temperature for SAMW formation properties in the Pacific and Indian Oceans. SOCAT $\Delta p\text{CO}_2$ values are primarily from narrow geographic regions in the Pacific sector near New Zealand and in the Indian sector near Tasmania. Biogeochemical Argo data are spread across the sectors, with more distributed density and potential temperature values as well. $\Delta p\text{CO}_2$ for SOCAT is similarly within relatively narrow ranges for both sectors, while Argo-derived $\Delta p\text{CO}_2$ overlaps with and, on average, is higher than SOCAT $\Delta p\text{CO}_2$. GLODAP-derived $\Delta p\text{CO}_2$ and associated properties are not shown, as they represent a much smaller sample range and were not included in the property averages (Table 2).

have difficulty in capturing the seasonal cycle of $p\text{CO}_2$ and air-sea CO_2 fluxes in the Southern Ocean (Mongwe et al., 2018). If the models do not accurately capture contemporary carbon uptake, then the anthropogenic carbon fluxes and storage will be biased.

Recent work attempting to constrain the magnitude of wintertime outgassing in the Southern Ocean (Bushinsky et al., 2019; Gray et al., 2018; Long et al., 2021; Mackay & Watson, 2021; Sutton et al., 2021) makes it all the more important to understand the mechanisms that could contribute to total Southern Ocean uptake of contemporary and anthropogenic carbon. A $\Delta p\text{CO}_2$ during formation that is near or above zero indicates that SAMW does not contribute to the total Southern Ocean contemporary carbon uptake during formation. Given the increase in atmospheric $p\text{CO}_2$ from anthropogenic emissions, it is likely that these waters would have been a pre-industrial source of carbon to the atmosphere and the current near-zero $\Delta p\text{CO}_2$ represents an anthropogenic carbon sink. It is clear from observed accumulation of anthropogenic carbon in the ocean interior (Gruber, Clement, et al., 2019; Mikaloff Fletcher et al., 2006; Sabine & Tanhua, 2010; Sabine et al., 2004) that SAMW is important for the storage of anthropogenic carbon and export to the ocean interior, but the modeling work that has sought to elucidate whether SAMW accumulates anthropogenic carbon through surface or interior processes has not had robust observations for validation (Groeskamp et al., 2016; Iudicone et al., 2011). Here we provide both the mean

biogeochemical properties and their distribution with respect to water mass density that can be used to validate model property distributions and representation of contemporary carbon fluxes, thereby improving future estimates of the magnitude and mechanisms of anthropogenic carbon uptake and partitioning of uptake between surface and interior processes.

3.4. Spatial and Interannual Variability of SAMW Formation Properties

Almost 15 years of Argo observations have provided invaluable information about strong interannual and spatial variability of SAMW physical properties. Argo observations have revealed that the strong wintertime MLD anomalies in the Pacific, Indian, and Atlantic sectors that develop in some years, and are associated with SAM and ENSO, tend to be out of phase in the western and eastern parts of ocean sectors (Cerovečki & Meijers, 2021; Meijers et al., 2019; Tamsitt et al., 2020). In years with anomalously strong formation of colder and denser varieties of SAMW in the eastern parts of the Indian and Pacific sectors, the formation of warmer and lighter varieties of SAMW in the western part of both ocean sectors is anomalously weak, enhancing the net cooling and densification in each ocean sector. Conditions reverse in years with the preferential formation of warmer and lighter varieties of SAMW (Cerovečki & Meijers, 2021). Anomalies that develop in the western part of one ocean sector can subsequently be advected by the ACC to arrive approximately 1 year later to the eastern SAMW formation region of the same ocean sector (Cerovečki et al., 2019; Meijers et al., 2019). This pattern of an east-west dipole in MLD anomalies and propagation of strong anomalies is evident in the BSOSE Aug-Sept time-mean MLD (Figure 6). During the 2013–2019 period of BSOSE model simulation analyzed here, the strongest MLD anomalies developed in 2016 when a strong El Niño event coincided with a strong positive SAM early in the year (Figure 6a). By austral winter 2016, both indexes transitioned to strongly negative (Meijers et al., 2019). The in-phase atmospheric modes resulted in anomalously deep and cold wintertime mixed layers in the central Pacific, and anomalously shallow and warm mixed layers in the southeast Pacific (Cerovečki et al., 2019; Meijers et al., 2019).

In addition to the previously described temperature anomalies (not shown) associated with the 2016 MLD anomalies, BSOSE displays high DIC and high NO_3^- in the central Pacific and low DIC and NO_3^- in the eastern Pacific (Figure 6b). The opposite pattern is observed in 2015, when anomalously shallow MLs in the central Pacific were associated with low DIC and low NO_3^- , while anomalously deep MLs in the eastern Pacific entrained high DIC and NO_3^- waters. These anomaly maps suggest a link between SAM, ENSO, and biogeochemical anomalies, but the BSOSE time series is too short for more definitive attribution in the current study. Due to this relatively short time period we chose to investigate interannual winter property anomalies rather than for example, carrying out an EOF analysis, though an initial EOF analysis produced qualitatively similar results.

A time-series of the wintertime (August–September) mean ML property anomalies within the Pacific SAMW density range ($26.8 \leq \sigma_\theta < 27.05 \text{ kg m}^{-3}$) considered separately in the central ($45\text{--}64^\circ\text{S}$, $170\text{--}246^\circ\text{E}$) and southeast ($45\text{--}64^\circ\text{S}$, $246\text{--}290^\circ\text{E}$) Pacific reveals a similar dipole pattern of DIC, nitrate, and oxygen as found in prior work considering physical properties (Figure 7). These two regions of the Pacific are not entirely out of phase, as the biogeochemical properties during the formation time period are not only governed by the local surface forcing that drives MLD anomalies, but also the properties from water formed in prior years incorporated through entrainment and lateral induction. The mean property anomalies of the Pacific are more closely correlated with central Pacific than the southeast Pacific due to the larger volume of water formed in the central Pacific, in agreement with observational work by Cerovečki and Meijers (2021).

Oxygen time variability is more complicated than that of nitrate and DIC, as the fast gas exchange rate moves to restore air-sea equilibrium and replenish waters that are initially deficient in oxygen but have low temperatures and high solubility. In some years, such as 2016 when the strong El Niño and strongly positive SAM combined to produce anomalously deep MLs in the central Pacific, the oxygen anomaly is negative, indicating that the entrainment signal was strong and persisted through the SAMW formation period (Figures 6 and 7). In other years, such as 2013, deep MLs in the central Pacific are associated with positive oxygen anomalies. This dichotomy reflects the competing processes that impact oxygen in the upper ocean. In years with strong heat loss to the atmosphere, cooler temperatures will increase the solubility, which, coupled with strong winds driving high air-sea gas exchange rates, will tend to increase the oxygen concentration in the surface ocean. On the other hand, deeper mixing will entrain more low-oxygen water from below and the increased volume of the mixed layer will slow the change in oxygen concentration for a given air-sea flux. Years with reduced air-sea heat loss in the winter

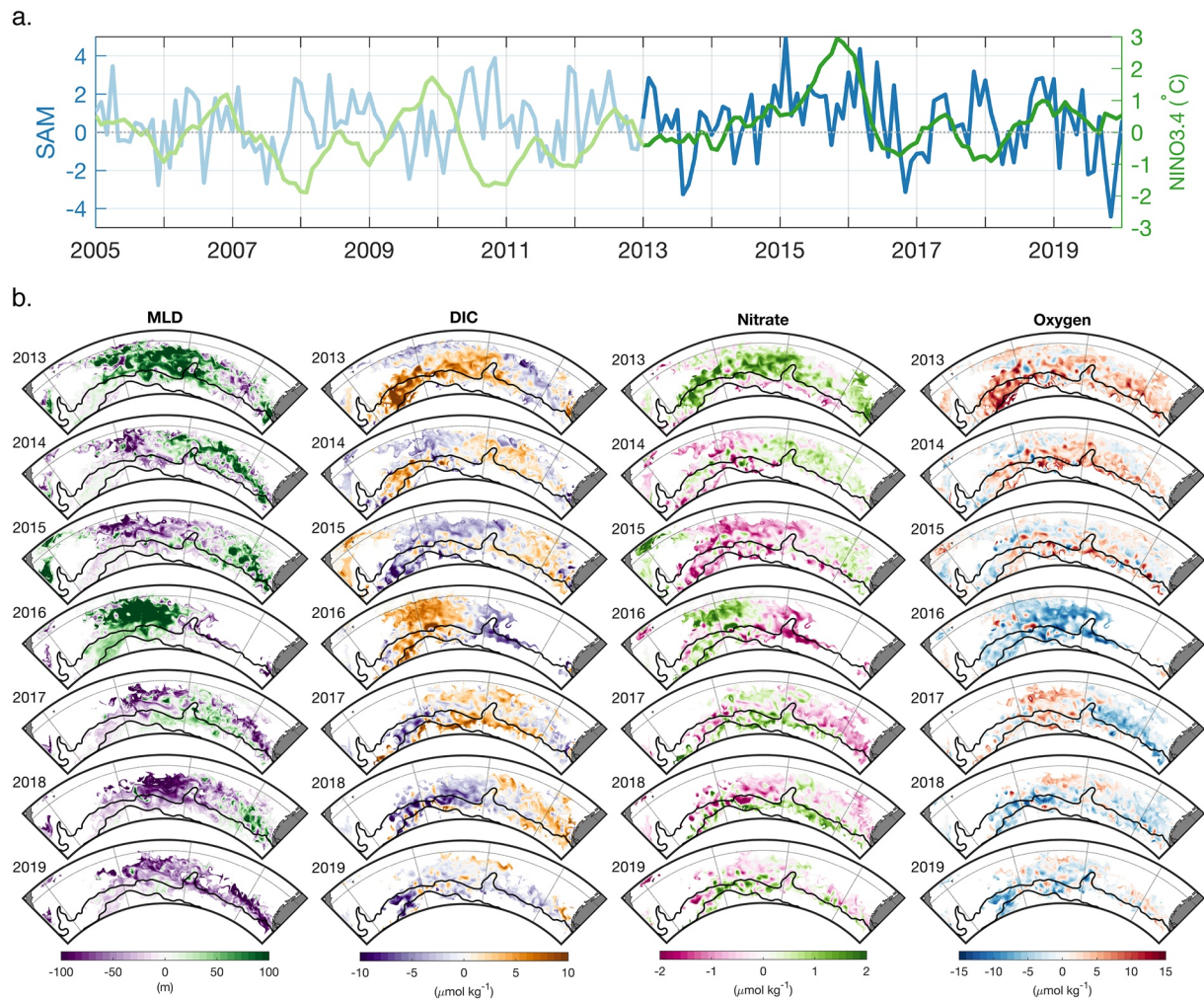


Figure 6. Time series of El Niño–Southern Oscillation (ENSO), Southern Annual Mode (SAM), and BSOSE winter anomalies in MLD, dissolved inorganic carbon (DIC), nitrate, and oxygen. (a) SAM (blue) and ENSO (green) indices are highlighted during the years covered by BSOSE. (b) Winter (August–September) anomalies for MLD, DIC, nitrate, and oxygen demonstrate the combined influence of ENSO and SAM. Years and regions with deep MLD anomalies (green) are associated with higher DIC (orange) and nitrate (green). Spatial patterns of anomalies demonstrate a dipole between the central Pacific and southeast Pacific in many years, similar to a previously demonstrated pattern in SST, and Salinity (Cerovečki & Meijers, 2021).

and shallower MLs are characterized by warmer temperatures and lower solubility but also less entrainment of low-oxygen waters. A plot of SAMW oxygen concentration against potential temperature for the Pacific and Pacific sub-regions reveals that the main signal is a fairly consistent offset relative to oxygen saturation of which approximately 1/3 is due to low SLP (Figure S4 in Supporting Information S1), implying that not only do oxygen concentrations closely follow interannual temperature changes, but also that the balance of the above processes leads to a consistent $\Delta[\text{O}_2]$ despite large changes in MLD and temperature. Both the magnitude of the $\Delta[\text{O}_2]$ offset and the lack of variability in BSOSE are consistent with float and ship-board observations (Figure 4) (Wolf et al., 2018).

Interestingly, the differences in biogeochemical property anomalies observed between the central and south-eastern Pacific are more pronounced during the first half of the BSOSE time series than after 2016 (Figure 7). Physical and biogeochemical properties across the Pacific become more uniform after the 2016 El Niño and remain so through 2017, 2018, and 2019 (Figure 7, difference between the central Pacific (red line, 45–64°S, 170–246°E), and southeast Pacific (blue line, 45–64°S, 246–290°E)). This is likely caused in part by advection of anomalies from the central to southeast Pacific following the strong 2016 El Niño, as previously shown for temperature anomalies using Argo data (Cerovečki & Meijers, 2021). Similar advection of anomalies of biogeochemical properties from west to east Pacific SAMW formation regions is evident in Figure 6. This propagation

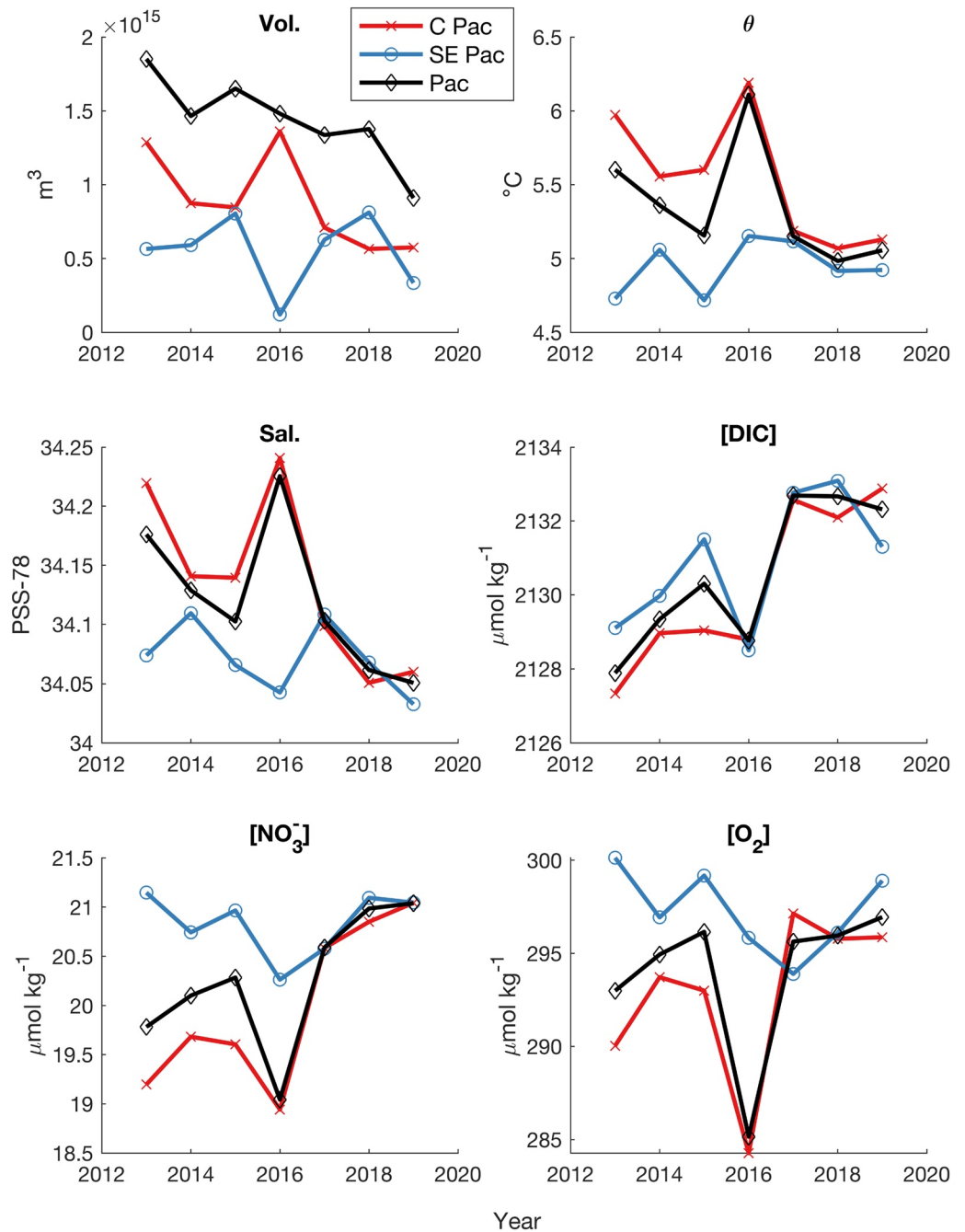


Figure 7. SAMW Pacific formation properties in BSOE. Anomalies are mean winter (August–September) ML properties in the Pacific SAMW density range ($26.8 \leq \sigma_{\theta} < 27.05 \text{ kg m}^{-3}$). Anomalies are calculated for the central (red line, $45\text{--}64^{\circ}\text{S}$, $170\text{--}246^{\circ}\text{E}$), southeast (blue, $45\text{--}64^{\circ}\text{S}$, $246\text{--}290^{\circ}\text{E}$), and overall Pacific (black, $45\text{--}64^{\circ}\text{S}$, $170\text{--}290^{\circ}\text{E}$) regions.

of signals across the entire Pacific formation region is suggested by the apparent movement of anomalies from west to east in Figure 6. Advection of biogeochemical anomalies in BSOE is more prominent when viewed in a Hovmöller diagram of the volume-weighted average upper ocean anomalies in the region where Aug–Sept MLs exceed 150 m (Figure S5 in Supporting Information S1). Similar advective signals have been described in Argo observations of physical properties (Cerovečki & Meijers, 2021) and previously in modeled temperature, salinity, and air-sea fluxes of oxygen and carbon dioxide (Verdy et al., 2007).

We are left with a framework where interannual variability in the biogeochemical properties of newly formed SAMW is influenced by a mix of local atmospheric forcing combined with the lateral induction of prior signals

into the wintertime mixed layer. This mix of processes agrees with prior work on SAMW physical properties (Cerovečki et al., 2019; Li et al., 2021; Meijers et al., 2019) and a study demonstrating that surface fluxes are often not strong enough to change the physical properties of SAMW, due to the memory in the large volume of sub-surface water (Rintoul & England, 2002). Advective propagation of anomalies can sometimes be interrupted by sufficiently large forcing events, but many biogeochemical anomalies do transit the entire Pacific SAMW formation region (Figure S5 in Supporting Information S1).

4. Conclusions

Here we use biogeochemical Argo float observations spanning a 7-year period to characterize for the first time the regional distribution of SAMW formation properties in the Pacific and Indian sectors, finding that the colder, fresher SAMW that forms in the Pacific is also higher in oxygen, nitrate, DIC, and $p\text{CO}_2$ than SAMW that forms in the Indian Ocean. The differences in formation properties between the Pacific and Indian Oceans reflect the density of SAMW formed in each region. The distribution of wintertime properties against density is consistent in both sectors, indicating that these property distributions predominantly represent a continuum of source water mass mixing between thermocline water, upwelled CDW, AAIW, and re-entrained SAMW.

In both the Pacific and Indian sectors, SAMW is undersaturated in oxygen at the time of formation, with slightly stronger undersaturation present in the Pacific formation regions. This undersaturation must be taken into account when calculating derived quantities that normally assume oxygen saturation at the time of water mass formation. This observed undersaturation appears fairly constant over the observed time period and matches results from biogeochemical ocean state estimate BSOSE that suggest some consistent balance between undersaturation due to cooling or entrainment and replenishment by air-sea gas exchange that is maintained despite large interannual differences in oxygen concentration and SST.

There are large differences between the mean $\Delta p\text{CO}_2$ of newly formed SAMW estimated from profiling floats and that measured by underway shipboard observations. Float estimates of winter $\Delta p\text{CO}_2$ are on average $\sim 17 \mu\text{atm}$ higher in this study than the limited SOCAT observations from the same formation regions, part of which could be due to a systemic bias in float-derived $p\text{CO}_2$. However, float observations are geographically more uniformly distributed over the SAMW formation regions, sampling a wider range of properties than has been measured from shipboard observations. The bulk of these differences can be explained by the different sample distribution in the two datasets. During the wintertime formation period, SAMW has a positive $\Delta p\text{CO}_2$ (average of SOCAT and float datasets) in the Pacific and a near neutral $\Delta p\text{CO}_2$ in the Indian formation region. This indicates that SAMW formation is not directly driving air-sea uptake of contemporary CO_2 . The biogeochemical observations here provide for the first time the comparison data necessary to determine if models used to understand how anthropogenic carbon enters the ocean interior through mode and intermediate waters are accurately representing ocean biogeochemistry during mode water formation.

There are sufficient float biogeochemical observations to constrain mean wintertime formation properties but there are not currently enough to investigate sub-regional or interannual variability. We thus used BSOSE output to explore spatial and temporal SAMW variability, focusing on the Pacific SAMW formation region. In the Pacific the link between climate modes of variability and SAMW response is the strongest and BSOSE representation of the spatial distribution of deep winter mixing in the Pacific was more similar to these from the RG-Argo than in the Indian sector. Comparison between this study and Cerovečki and Meijers (2021) indicates that BSOSE well reproduces the large-scale response of the MLD to SAM and ENSO, showing the dipole pattern of variability between the central and southeast Pacific. BSOSE also accurately represents the relationships between biogeochemical properties and water mass density that we find in observations, giving good confidence that it can be used to develop our understanding of the link between climate forcing and biogeochemical property variability in SAMW formation waters.

Interannual variability in the central and southeast Pacific biogeochemical formation properties displays a see-saw pattern similar to that previously found in observations of physical properties. The suggested dipole pattern of biogeochemical properties relates well to the corresponding pattern in MLD and entrainment of deeper waters, with high nitrate and high DIC in regions and years with deep mixed layer anomalies and low nitrate and low DIC when the mixed layer is anomalously shallow. We expect that with more biogeochemical observations made in the Southern Ocean, these patterns will become evident in the observations as well. Interannual variability in

oxygen concentration closely follows changes in ML temperature with a consistent undersaturation indicating that ML waters do not have time to equilibrate with the atmosphere regardless of whether the MLDs are anomalously deep or shallow.

Future work should focus on decomposing interannual variability in biogeochemical signals between those driven by local forcing and the influence of multi-year advective signals. A detailed understanding of the variability present in SAMW formation regions will help to determine how sensitive the interior volume is to changes in volume and properties of the individual formation regions and how strongly those variations are either modulated by the total interior SAMW volume or transported to the rest of the ocean.

SAMW is a critical water mass for the uptake of anthropogenic carbon and transport of oxygen and nutrients into the ocean interior. Improving our understanding of SAMW biogeochemical properties and their variability is of fundamental importance for improving our interpretation of interior ocean measurements, providing better validation for models, and therefore enabling new understanding of how SAMW functions in these global biogeochemical cycles.

Conflict of Interest

The authors declare no conflicts of interest relevant to this study.

Data Availability Statement

Datasets used in this paper are from these references and the associated repositories: Biogeochemical float data are from the May 2021 SOCCOM snapshot (Johnson et al., 2017; <https://doi.org/10.6075/J0T43SZG>), along with the Drucker and Riser (2016) UW Argo Oxygen data set which is now included in the Argo data set (<https://argo.ucsd.edu/data/data-from-gdacs/>). Gridded Argo product by Roemmich and Gilson (2009) is available from <https://argo.ucsd.edu/data/argo-data-products/>. Argo data were collected and made freely available by the International Argo Program and the national programs that contribute to it (<http://doi.org/10.17882/42182>, <http://www.argo.ucsd.edu>, <http://argo.jcommops.org>). Shipboard data are from SOCAT v2021 (Bakker et al., 2016; <https://www.socat.info/index.php/data-access/>) and GLODAP v2.2020 (Key et al., 2015; Olsen et al., 2016; <https://www.glodap.info/index.php/merged-and-adjusted-data-product/>). Analysis and plotting code for this study are available at <https://doi.org/10.5281/zenodo.7349405> (Bushinsky & Cerovečki, 2022).

References

- Álvarez, M., Lo Monaco, C., Tanhua, T., Yool, A., Oschlies, A., Bullister, J. L., et al. (2009). Estimating the storage of anthropogenic carbon in the subtropical Indian Ocean: A comparison of five different approaches. *Biogeosciences*, 6(4), 681–703. <https://doi.org/10.5194/bg-6-681-2009>
- Bakker, D. C. E., Pfeil, B., Landa, C. S., Metzl, N., O'Brien, K. M., Olsen, A., et al. (2016). A multi-decade record of high-quality fCO₂ data in version 3 of the Surface Ocean CO₂ Atlas (SOCAT). *Earth System Science Data*, 8(2), 383–413. <https://doi.org/10.5194/essd-8-383-2016>
- Broecker, W. S., & Peng, T. H. (1982). *Tracers in the sea*. Lamont-Doherty Earth Observatory.
- Bushinsky, S., & Cerovečki, I. (2022). Subantarctic Mode Water Biogeochemical Formation Properties and Interannual Variability, analysis and plotting code (v1.1.1). <https://doi.org/10.5281/zenodo.7349405>
- Bushinsky, S. M., Gray, A. R., Johnson, K. S., & Sarmiento, J. L. (2017). Oxygen in the Southern Ocean from Argo floats: Determination of processes driving air-sea fluxes. *Journal of Geophysical Research: Ocean*, 122(11), 8661–8682. <https://doi.org/10.1002/2017JC012923>
- Bushinsky, S. M., Landschützer, P., Rödenbeck, C., Gray, A. R., Baker, D., Mazloff, M. R., et al. (2019). Reassessing southern ocean air-sea CO₂ Flux estimates with the addition of biogeochemical float observations. *Global Biogeochemical Cycles*, 33(11), 1370–1388. <https://doi.org/10.1029/2019GB006176>
- Carter, B. R., Feely, R. A., Lauvset, S. K., Olsen, A., DeVries, T., & Sonnerup, R. (2021). Preformed properties for marine organic matter and carbonate mineral cycling quantification. *Global Biogeochemical Cycles*, 35(1), 64–75. <https://doi.org/10.1029/2020GB006623>
- Carter, B. R., Feely, R. A., Williams, N. L., Dickson, A. G., Fong, M. B., & Takeshita, Y. (2018). Updated methods for global locally interpolated estimation of alkalinity, pH, and nitrate. *Limnology and Oceanography: Methods*, 16(2), 119–131. <https://doi.org/10.1002/lom3.10232>
- Carter, B. R., Talley, L. D., & Dickson, A. G. (2014). Mixing and remineralization in waters detrain from the surface into Subantarctic Mode Water and Antarctic intermediate water in the southeastern Pacific. *Journal of Geophysical Research Oceans*, 119(6), 4001–4028. <https://doi.org/10.1002/2013JC009355>
- Cerovečki, I., & Mazloff, M. R. (2016). The spatiotemporal structure of diabatic processes governing the evolution of Subantarctic Mode Water in the southern ocean. *Journal of Physical Oceanography*, 46(2), 683–710. <https://doi.org/10.1175/JPO-D-14-0243.1>
- Cerovečki, I., & Meijers, A. J. S. (2021). Strong quasi-stationary wintertime atmospheric surface pressure anomalies drive a dipole pattern in the Subantarctic Modewater Formation. *Journal of Climate*, 1–44. <https://doi.org/10.1175/JCLI-D-20-0593.1>
- Cerovečki, I., Meijers, A. J. S., Mazloff, M. R., Gille, S. T., Tamsitt, V. M., & Holland, P. R. (2019). The effects of enhanced sea ice export from the Ross Sea on recent cooling and freshening of the southeast Pacific. *Journal of Climate*, 32(7), 2013–2035. <https://doi.org/10.1175/JCLI-D-18-0205.1>

Acknowledgments

Float data were collected and made freely available by the Southern Ocean Carbon and Climate Observations and Modeling (SOCCOM) Project funded by the National Science Foundation, Division of Polar Programs (NSF PLR -1425989 and OPP-1936222), supplemented by NASA, and by the International Argo Program and the NOAA programs that contribute to it. The Argo Program is part of the Global Ocean Observing System. The Surface Ocean CO₂ Atlas (SOCAT) is an international effort, endorsed by the International Ocean Carbon Coordination Project (IOCCP), the Surface Ocean Lower Atmosphere Study (SOLAS) and the Integrated Marine Biosphere Research (IMBeR) program, to deliver a uniformly quality-controlled surface ocean CO₂ database. The many researchers and funding agencies responsible for the collection of data and quality control are thanked for their contributions to SOCAT. The specific SOCAT data used in this study were contributed by PIs K. Currie, A. Sutton, T. Trull, C. Sabine, T. Takahashi, C. Sweeney, S. C. Sutherland, T. Newberger, D. R. Munro, B. Tilbrook, J. Akl, and C. Neill. SOCAT data from the R/V Tangaroa were collected by the National Institute of Water and Atmospheric Research (funded by the New Zealand Ministry of Business, Innovation and Employment). SOCAT data from the R/V Gould and R/V Palmer were funded by the National Oceanic and Atmospheric Administration through the Global Ocean Monitoring and Observing Program and the Office of Oceanic and Atmospheric Research and by the National Science Foundation (Grants PLR 1341647 and 1543457). SOCAT underway data from Tilbrook, Akl and Neill were sourced through Australia's Integrated Marine Observing System (IMOS)—IMOS is enabled by the National Collaborative Research Infrastructure Strategy (NCRIS). Specific GLODAP data were collected on the R/Vs Knorr, Aurora Australis, Malcolm Baldrige, and M.-Dufresne. SMB was supported by NASA Grants NNX17AI73G and 80NSSC22K0156 and benefited from support by the NOAA Climate Program Office's Climate Observations and Monitoring, Climate Variability and Predictability, and Global Ocean Monitoring and Observation programs (NA21OAR4310260). IC was supported by NASA Grants 80NSSC22K0156 and 80NSSC19K1115. This is SOEST contribution 11625.

- de Boyer Montégut, C., Madec, G., Fischer, A. S., Lazar, A., & Iudicone, D. (2004). Mixed layer depth over the global ocean: An examination of profile data and a profile-based climatology. *Journal of Geophysical Research*, *109*(C12), C12003. <https://doi.org/10.1029/2004JC002378>
- Dee, D. P., Uppala, S. M., Simmons, A. J., Berrisford, P., Poli, P., Kobayashi, S., et al. (2011). The ERA-Interim reanalysis: Configuration and performance of the data assimilation system. *Quarterly Journal of the Royal Meteorological Society*, *137*(656), 553–597. <https://doi.org/10.1002/qj.828>
- DeVries, T. (2014). The oceanic anthropogenic CO₂ sink: Storage, air-sea fluxes, and transports over the industrial era. *Global Biogeochemical Cycles*, *28*(7), 631–647. <https://doi.org/10.1002/2013GB004739>
- Dlugokencky, E. J., Thoning, K. W., Lang, P. M., & Tans, P. P. (2019). NOAA greenhouse gas reference from atmospheric carbon dioxide dry air mole fractions from the NOAA ESRL carbon cycle cooperative global air sampling network.
- Downes, S. M., Langlais, C., Brook, J. P., & Spence, P. (2017). Regional impacts of the westerly winds on Southern Ocean mode and intermediate water subduction. *Journal of Physical Oceanography*, *47*(10), 2521–2530. <https://doi.org/10.1175/JPO-D-17-0106.1>
- Drucker, R., & Riser, S. C. (2016). In situ phase-domain calibration of oxygen Optodes on profiling floats. *Methods in Oceanography*, *17*, 1–34. <https://doi.org/10.1016/j.mio.2016.09.007>
- Duteil, O., Koeve, W., Oschlies, A., Bianchi, D., Galbraith, E., Kriest, I., & Mear, R. (2013). A novel estimate of ocean oxygen utilisation points to a reduced rate of respiration in the ocean interior. *Biogeosciences*, *10*(11), 7723–7738. <https://doi.org/10.5194/bg-10-7723-2013>
- Fay, A. R., Lovenduski, N. S., McKinley, G. A., Munro, D. R., Sweeney, C., Gray, A. R., et al. (2018). Utilizing the Drake Passage time-series to understand variability and change in subpolar Southern Ocean pCO₂. *Biogeosciences Discussions*, *15*(12), 3841–3855. <https://doi.org/10.5194/bg-2017-489>
- Fay, A. R., McKinley, G. A., & Lovenduski, N. S. (2014). Southern Ocean carbon trends: Sensitivity to methods. *Geophysical Research Letters*, *41*(19), 6833–6840. <https://doi.org/10.1002/2014GL061324>
- Fernández Castro, B., Mazloff, M., Williams, R. G., & Naveira Garabato, A. C. (2022). Subtropical contribution to sub-Antarctic mode waters. *Geophysical Research Letters*, *49*(11), e2021GL097560. <https://doi.org/10.1029/2021gl097560>
- Gao, L., Rintoul, S. R., & Yu, W. (2018). Recent wind-driven change in Subantarctic Mode Water and its impact on ocean heat storage. *Nature Climate Change*, *8*(1), 58–63. <https://doi.org/10.1038/s41558-017-0022-8>
- García, H. E., & Gordon, L. I. (1992). Oxygen solubility in seawater: Better fitting equations. *Limnology & Oceanography*, *37*(6), 1307–1312. <https://doi.org/10.4319/lo.1992.37.6.1307>
- García, H. E., Locarnini, R. A., Boyer, T. P., Levitus, S., & Locarnini, R. A. (2010). World Ocean Atlas 2009 volume 3: Dissolved oxygen, apparent oxygen utilization, and oxygen saturation.
- Gray, A. R., Johnson, K. S., Bushinsky, S. M., Riser, S. C., Russell, J. L., Talley, L. D., et al. (2018). Autonomous biogeochemical floats detect significant carbon dioxide outgassing in the high-latitude southern Ocean. *Geophysical Research Letters*, *45*(17), 9049–9057. <https://doi.org/10.1029/2018GL078013>
- Groeskamp, S., Lenton, A., Mear, R., Sloyan, B. M., & Langlais, C. (2016). Anthropogenic carbon in the ocean—Surface to interior connections. *Global Biogeochemical Cycles*, *30*(11), 1682–1698. <https://doi.org/10.1002/2016GB005476>
- Gruber, N., Clement, D., Carter, B. R., Feely, R. A., van Heuven, S., Hoppema, M., et al. (2019). The oceanic sink for anthropogenic CO₂ from 1994 to 2007. *Science*, *363*(6432), 1193–1199. <https://doi.org/10.1126/science.aau5153>
- Gruber, N., Doney, S. C., Emerson, S. R., Gilbert, D., Kobayashi, T., Körtzinger, A., et al. (2009). Adding oxygen to Argo: Developing a global in-situ observatory for ocean deoxygenation and biogeochemistry. *Ocean Obs '09*.
- Gruber, N., Gloor, M., Mikaloff Fletcher, S. E., Doney, S. C., Dutkiewicz, S., Follows, M. J., et al. (2009). Oceanic sources, sinks, and transport of atmospheric CO₂. *Global Biogeochemical Cycles*, *23*(1), GB1005. <https://doi.org/10.1029/2008GB003349>
- Gruber, N., Landschützer, P., & Lovenduski, N. S. (2019). The variable Southern Ocean Carbon sink. *Annual Review of Marine Science*, *11*(1), 159–186. <https://doi.org/10.1146/annurev-marine-121916-063407>
- Hanawa, K., & Talley, L. (2001). Mode waters. In *International geophysics* (pp. 373–386).
- Hartin, C. A., Fine, R. A., Sloyan, B. M., Talley, L. D., Chereskin, T. K., & Happell, J. (2011). Formation rates of Subantarctic Mode Water and Antarctic intermediate water within the South Pacific. *Deep-Sea Research Part I: Oceanographic Research Papers*, *58*(5), 524–534. <https://doi.org/10.1016/j.dsr.2011.02.010>
- Herraiz-Borreguero, L., & Rintoul, S. R. (2011). Subantarctic Mode Water: Distribution and circulation. *Ocean Dynamics*, *61*(1), 103–126. <https://doi.org/10.1007/s10236-010-0352-9>
- Ito, T., Follows, M. J., & Boyle, E. A. (2004). Is AOU a good measure of respiration in the oceans? *Geophysical Research Letters*, *31*(17), L17305. <https://doi.org/10.1029/2004GL020900>
- Iudicone, D., Rodgers, K. B., Plancherel, Y., Aumont, O., Ito, T., Key, R. M., et al. (2016). The formation of the ocean's anthropogenic carbon reservoir. *Scientific Reports*, *6*(1), 35473. <https://doi.org/10.1038/srep35473>
- Iudicone, D., Rodgers, K. B., Stando, I., Aumont, O., Madec, G., Bopp, L., et al. (2011). Water masses as a unifying framework for understanding the Southern Ocean Carbon Cycle. *Biogeosciences*, *8*(5), 1031–1052. <https://doi.org/10.5194/bg-8-1031-2011>
- Johnson, K. S., Plant, J. N., Coletti, L. J., Jannasch, H. W., Sakamoto, C. M., Riser, S. C., et al. (2017). Biogeochemical sensor performance in the SOCCOM profiling float array. *Journal of Geophysical Research: Ocean*, *122*(8), 6416–6436. <https://doi.org/10.1002/2017JC012838>
- Kalnay, E., Kanamitsu, M., Kistler, R., Collins, W., Deaven, D., Gandin, L., et al. (1996). The NCEP/NCAR 40-year reanalysis project. *Bulletin of the American Meteorological Society*, *77*(3), 437–471. [https://doi.org/10.1175/1520-0477\(1996\)077<0437:TNYRP>2.0.CO;2](https://doi.org/10.1175/1520-0477(1996)077<0437:TNYRP>2.0.CO;2)
- Key, R. M., Olsen, A., van Heuven, S., Lauvset, S. K., Velo, A., Lin, X., et al. (2015). Global Ocean Data Analysis Project, Version 2 (GLODAPv2). ORNL/CDIAC-162, NDP-093. https://doi.org/10.3334/CDIAC/OTG.NDP093_GLODAPv2
- Koch-Larrouy, A., Morrow, R., Penduff, T., & Juza, M. (2010). Origin and mechanism of Subantarctic Mode Water formation and transformation in the southern Indian Ocean. *Ocean Dynamics*, *60*(3), 563–583. <https://doi.org/10.1007/s10236-010-0276-4>
- Koeve, W., & Kähler, P. (2016). Oxygen utilization rate (OUR) underestimates ocean respiration: A model study. *Global Biogeochemical Cycles*, *30*(8), 1166–1182. <https://doi.org/10.1002/2015GB005354>
- Kolodziejczyk, N., Llovel, W., & Portela, E. (2019). Interannual variability of upper ocean water masses as inferred from Argo array. *Journal of Geophysical Research Oceans*, *124*(8), 6067–6085. <https://doi.org/10.1029/2018JC014866>
- Landschützer, P., Gruber, N., & Bakker, D. C. E. (2016). Decadal variations and trends of the global ocean carbon sink. *Global Biogeochemical Cycles*, *30*(10), 1396–1417. <https://doi.org/10.1002/2015GB005359>
- Landschützer, P., Gruber, N., Bakker, D. C. E., Schuster, U., Nakaoka, S., Payne, M. R., et al. (2013). A neural network-based estimate of the seasonal to inter-annual variability of the Atlantic Ocean carbon sink. *Biogeosciences*, *10*(11), 7793–7815. <https://doi.org/10.5194/bg-10-7793-2013>
- Landschützer, P., Gruber, N., Haumann, F. A., Rödenbeck, C., Bakker, D. C. E., van Heuven, S., et al. (2015). The reinvigoration of the Southern Ocean carbon sink. *Science*, *349*(6253), 1221–1224. <https://doi.org/10.1126/science.aab2620>

- Lauvset, S., Currie, K., Metzl, N., Nakaoka, S. I., Bakker, D., Sullivan, K., et al. (2017). SOCAT quality control cookbook: For SOCAT version 7. *SOCAT*. <https://doi.org/10.25607/OBP-1665>
- Lauvset, S. K., Key, R. M., Olsen, A., van Heuven, S., Velo, A., Lin, X., et al. (2016). A new global interior ocean mapped climatology: The $1^\circ \times 1^\circ$ GLODAP version 2. *Earth System Science Data*, 8, 325–340. <https://doi.org/10.5194/essd-8-325-2016>
- Lenton, A., & Mearns, R. J. (2007). Role of the Southern Annular Mode (SAM) in southern Ocean CO₂ uptake. *Global Biogeochemical Cycles*, 21(2), 1–17. <https://doi.org/10.1029/2006GB002714>
- Li, Z., England, M. H., Groeskamp, S., Cerovečki, I., & Luo, Y. (2021). The origin and fate of Subantarctic Mode Water in the Southern Ocean. *Journal of Physical Oceanography*, 2951–2972. <https://doi.org/10.1175/jpo-d-20-0174.1>
- Long, M. C., Stephens, B. B., McKain, K., Sweeney, C., Keeling, R. F., Kort, E. A., et al. (2021). Strong Southern Ocean carbon uptake evident in airborne observations. *Science*, 374(6572), 1275–1280. <https://doi.org/10.1126/science.abi4355>
- Lovenduski, N. S., Gruber, N., Doney, S. C., & Lima, I. D. (2007). Enhanced CO₂ outgassing in the Southern Ocean from a positive phase of the southern annular mode. *Global Biogeochemical Cycles*, 21, GB2026. <https://doi.org/10.1029/2006GB002900>
- Mackay, N., & Watson, A. (2021). Winter air-sea CO₂ fluxes constructed from summer observations of the Polar Southern Ocean suggest weak outgassing. *Journal of Geophysical Research: Ocean*, 126(5), e2020JC016600. <https://doi.org/10.1029/2020jc016600>
- Maurer, T. L., Plant, J. N., & Johnson, K. S. (2021). Delayed-mode quality control of oxygen, nitrate, and pH Data on SOCCOM biogeochemical profiling floats. *Frontiers in Marine Science*, 8, 1–20. <https://doi.org/10.3389/fmars.2021.683207>
- McCartney, M. (1982). The subtropical recirculation of mode waters. *Journal of Marine Research*, 40, 427–464.
- McCartney, M. S. (1977). Subantarctic Mode Water. In M. Angel (Ed.), *A voyage of discovery: George deacon 70th anniversary* (pp. 103–119).
- Meijers, A. J. S., Cerovečki, I., King, B. A., & Tamsitt, V. (2019). A see-saw in Pacific Subantarctic Mode Water formation driven by atmospheric modes. *Geophysical Research Letters*, 46(22), 13152–13160. <https://doi.org/10.1029/2019GL085280>
- Mikaloff Fletcher, S. E., Gruber, N., Jacobson, A. R., Doney, S. C., Dutkiewicz, S., Gerber, M., et al. (2006). Inverse estimates of anthropogenic CO₂ uptake, transport, and storage by the ocean. *Global Biogeochemical Cycles*, 20, GB2002. <https://doi.org/10.1029/2005GB002530>
- Mikaloff Fletcher, S. E., Gruber, N., Jacobson, A. R., Gloor, M., Doney, S. C., Dutkiewicz, S., et al. (2007). Inverse estimates of the oceanic sources and sinks of natural CO₂ and the implied oceanic carbon transport. *Global Biogeochemical Cycles*, 21, 1–19. <https://doi.org/10.1029/2006GB002751>
- Mongwe, N. P., Vichi, M., & Monteiro, P. M. S. (2018). The seasonal cycle of pCO₂ and CO₂ fluxes in the Southern Ocean: Diagnosing anomalies in CMIP5 Earth system models. *Biogeosciences*, 15(9), 2851–2872. <https://doi.org/10.5194/bg-15-2851-2018>
- Morrison, A. K., Frölicher, T. L., & Sarmiento, J. L. (2015). Upwelling in the Southern Ocean. *Physics Today*, 68(1), 27–32. <https://doi.org/10.1063/PT.3.2654>
- Morrison, A. K., Waugh, D. W., Hogg, A. M., Jones, D. C., & Abernathy, R. P. (2022). Ventilation of the Southern Ocean pycnocline. *Annual Review of Marine Science*, 14(1), 405–430. <https://doi.org/10.1146/annurev-marine-010419-011012>
- Olsen, A., Key, R. M., Van Heuven, S., Lauvset, S. K., Velo, A., Lin, X., et al. (2016). The global ocean data analysis project version 2 (GLODAPv2)—An internally consistent data product for the World Ocean. *Earth System Science Data*, 8, 297–323. <https://doi.org/10.5194/essd-8-297-2016>
- Orsi, A. H., Whitworth, T., & Nowlin, W. D. (1995). On the meridional extent and fronts of the Antarctic circumpolar current. *Deep Sea Research Part I: Oceanographic Research Papers*, 42(5), 641–673. [https://doi.org/10.1016/0967-0637\(95\)00021-W](https://doi.org/10.1016/0967-0637(95)00021-W)
- Portela, E., Kolodziejczyk, N., Maes, C., & Thierry, V. (2020). Interior water-mass variability in the southern hemisphere oceans during the last decade. *Journal of Physical Oceanography*, 50(2), 361–381. <https://doi.org/10.1175/JPO-D-19-0128.1>
- Primeau, F. W., Holzer, M., & DeVries, T. (2013). Southern Ocean nutrient trapping and the efficiency of the biological pump. *Journal of Geophysical Research Oceans*, 118(5), 2547–2564. <https://doi.org/10.1002/jgrc.20181>
- Qu, T., Gao, S., & Fine, R. A. (2020). Variability of the sub-Antarctic mode water subduction rate during the Argo period. *Geophysical Research Letters*, 47(13), e2020GL088248. <https://doi.org/10.1029/2020GL088248>
- Raphael, M. N. (2004). A zonal wave 3 index for the Southern Hemisphere. *Geophysical Research Letters*, 31(23), 1–4. <https://doi.org/10.1029/2004GL020365>
- Rintoul, S. R., & England, M. H. (2002). Ekman transport dominates local air-sea fluxes in driving variability of Subantarctic Mode Water. *Journal of Physical Oceanography*, 32(5), 1308–1321. [https://doi.org/10.1175/1520-0485\(2002\)032<1308:ETDLAS>2.0.CO;2](https://doi.org/10.1175/1520-0485(2002)032<1308:ETDLAS>2.0.CO;2)
- Rödenbeck, C., Keeling, R. F., Bakker, D. C. E., Metzl, N., Olsen, A., Sabine, C., & Heimann, M. (2013). Global surface-ocean pCO₂ and sea-air CO₂ flux variability from an observation-driven ocean mixed-layer scheme. *Ocean Science*, 9(2), 193–216. <https://doi.org/10.5194/os-9-193-2013>
- Roemmich, D., & Gilson, J. (2009). The 2004–2008 mean and annual cycle of temperature, salinity, and steric height in the global ocean from the Argo Program. *Progress in Oceanography*, 82(2), 81–100. <https://doi.org/10.1016/j.pocean.2009.03.004>
- Russell, J. L., & Dickson, A. G. (2003). Variability in oxygen and nutrients in south Pacific Antarctic intermediate water. *Global Biogeochemical Cycles*, 17(2), 1033. <https://doi.org/10.1029/2000GB001317>
- Sabine, C. L., Feely, R. A., Gruber, N., Key, R. M., Lee, K., Bullister, J. L., et al. (2004). The Oceanic sink for anthropogenic CO₂. *Science*, 305(5682), 367–371. <https://doi.org/10.1126/science.1097403>
- Sabine, C. L., & Tanhua, T. (2010). Estimation of anthropogenic CO₂ inventories in the Ocean. *Annual Review of Marine Science*, 2(1), 175–198. <https://doi.org/10.1146/annurev-marine-120308-080947>
- Sallée, J. B., Speer, K. G., & Rintoul, S. R. (2010). Zonally asymmetric response of the Southern Ocean mixed-layer depth to the southern annular mode. *Nature Geoscience*, 3(4), 273–279. <https://doi.org/10.1038/ngeo812>
- Sarmiento, J. L., Gruber, N., Brzezinski, M. A., & Dunne, J. P. (2004). High-latitude controls of thermocline nutrients and low latitude biological productivity. *Nature*, 427(7374), 56–60. <https://doi.org/10.1038/nature10605>
- Sloyan, B. M., & Rintoul, S. R. (2001). The Southern Ocean limb of the global deep overturning circulation*. *Journal of Physical Oceanography*, 31(1), 143–173. [https://doi.org/10.1175/1520-0485\(2001\)031<0143:TSOLOT>2.0.CO;2](https://doi.org/10.1175/1520-0485(2001)031<0143:TSOLOT>2.0.CO;2)
- Speer, K., Rintoul, S. R., & Sloyan, B. (2000). The diabatic deacon cell*. *Journal of Physical Oceanography*, 30(12), 3212–3222. [https://doi.org/10.1175/1520-0485\(2000\)030<3212:TDDC>2.0.CO;2](https://doi.org/10.1175/1520-0485(2000)030<3212:TDDC>2.0.CO;2)
- Sutton, A. J., Williams, N. L., & Tilbrook, B. (2021). Constraining Southern Ocean CO₂ flux uncertainty using uncrewed surface vehicle observations. *Geophysical Research Letters*, 48(3), 1–9. <https://doi.org/10.1029/2020GL091748>
- Tamsitt, V., Cerovečki, I., Josey, S. A., Gille, S. T., & Schulz, E. (2020). Mooring observations of air-sea heat fluxes in two Subantarctic Mode Water formation regions. *Journal of Climate*, 33(7), 2757–2777. <https://doi.org/10.1175/JCLI-D-19-0653.1>
- van Heuven, S. M. A. C., Pierrot, D., Rae, J. W. B., Lewis, E., & Wallace, D. W. R. (2011). Matlab program developed for CO₂ system calculations (p. 530).

- Verdy, A., Dutkiewicz, S., Follows, M. J., Marshall, J., & Czaja, A. (2007). Carbon dioxide and oxygen fluxes in the Southern Ocean: Mechanisms of interannual variability. *Global Biogeochemical Cycles*, 21(2), 1–10. <https://doi.org/10.1029/2006GB002916>
- Verdy, A., & Mazloff, M. R. (2017). A data assimilating model for estimating Southern Ocean biogeochemistry. *Journal of Geophysical Research: Oceans*, 122(9), 1–22. <https://doi.org/10.1002/2016JC012650>
- Williams, N. L., Juranek, L. W., Feely, R. A., Johnson, K. S., Sarmiento, J. L., Talley, L. D., et al. (2017). Calculating surface ocean $p\text{CO}_2$ from biogeochemical Argo floats equipped with pH: An uncertainty analysis. *Global Biogeochemical Cycles*, 31(3), 591–604. <https://doi.org/10.1002/2016GB005541>
- Williams, N. L., Juranek, L. W., Feely, R. A., Russell, J. L., Johnson, K. S., & Hales, B. (2018). Assessment of the carbonate chemistry seasonal cycles in the Southern Ocean from persistent observational platforms. *Journal of Geophysical Research: Oceans*, 123(7), 1–20. <https://doi.org/10.1029/2017JC012917>
- Wolf, M. K., Hamme, R. C., Gilbert, D., Yashayaev, I., & Thierry, V. (2018). Oxygen saturation surrounding deep water formation events in the Labrador Sea from Argo- O_2 data. *Global Biogeochemical Cycles*, 32(4), 635–653. <https://doi.org/10.1002/2017GB005829>
- Wong, A. P. S., Bindoff, N. L., & Church, J. A. (1999). Large-scale freshening of intermediate waters in the Pacific and Indian oceans. *Nature*, 400(6743), 440–443. <https://doi.org/10.1038/22733>
- Wu, Y., Bakker, D. C. E., Achterberg, E. P., Silva, A. N., Pickup, D. D., Li, X., et al. (2022). Integrated analysis of carbon dioxide and oxygen concentrations as a quality control of ocean float data. *Communications Earth & Environment*, 3(1), 92. <https://doi.org/10.1038/s43247-022-00421-w>
- Zeebe, R. E., & Wolf-Gladrow, D. A. (2001). *CO₂ in seawater: Equilibrium, kinetics, isotopes*. Elsevier.